



HAL
open science

The F-box protein UFO controls flower development by redirecting the master transcription factor LEAFY to new cis-elements

Philippe Rieu, Laura Turchi, Emmanuel Thévenon, Eleftherios Zarkadas, Max Nanao, Hicham Chahtane, Gabrielle Tichtinsky, Jérémy Lucas, Romain Blanc-Mathieu, Chloe Zubieta, et al.

► To cite this version:

Philippe Rieu, Laura Turchi, Emmanuel Thévenon, Eleftherios Zarkadas, Max Nanao, et al.. The F-box protein UFO controls flower development by redirecting the master transcription factor LEAFY to new cis-elements. *Nature Plants*, 2023, 9 (2), pp.315-329. 10.1038/s41477-022-01336-2. hal-03993820

HAL Id: hal-03993820

<https://cnrs.hal.science/hal-03993820>

Submitted on 17 Feb 2023

HAL is a multi-disciplinary open access archive for the deposit and dissemination of scientific research documents, whether they are published or not. The documents may come from teaching and research institutions in France or abroad, or from public or private research centers.

L'archive ouverte pluridisciplinaire **HAL**, est destinée au dépôt et à la diffusion de documents scientifiques de niveau recherche, publiés ou non, émanant des établissements d'enseignement et de recherche français ou étrangers, des laboratoires publics ou privés.

1 **Title**

2

3 The F-box protein UFO controls flower development by redirecting the master transcription
4 factor LEAFY to novel cis-elements

5

6

7 **Authors**

8

9 Philippe Rieu¹, Laura Turchi^{1,2}, Emmanuel Thévenon¹, Eleftherios Zarkadas^{3,4}, Max Nanao⁵,
10 Hicham Chahtane^{1,†}, Gabrielle Tichtinsky¹, Jérémy Lucas¹, Romain Blanc-Mathieu¹, Chloe
11 Zubieta¹, Guy Schoehn³, François Parcy^{1*}

12

13 **Affiliations**

14

15 ¹ Univ. Grenoble Alpes, CEA, CNRS, INRAE, Laboratoire Physiologie Cellulaire et Végétale,
16 IRIG-DBSCI-LPCV, Grenoble, France

17 ² Univ. Grenoble Alpes, CNRS, Translational Innovation in Medicine and Complexity,
18 Grenoble, France

19 ³ Univ. Grenoble Alpes, CNRS, CEA, IBS, F-38000 Grenoble, France

20 ⁴ Univ. Grenoble Alpes, CNRS, CEA, EMBL, ISBG, F-38000 Grenoble, France

21 ⁵ European Synchrotron Radiation Facility, Structural Biology, Group, Grenoble, France

22 † Present address: Institut de Recherche Pierre Fabre, Green Mission Pierre Fabre,
23 Conservatoire Botanique Pierre Fabre, Soual, France.

24 * Corresponding author. Email: francois.parcy@cea.fr

25

26

27 **Abstract**

28

29 In angiosperms, flower development requires the combined action of the transcription factor
30 (TF) LEAFY (LFY), and the ubiquitin ligase adaptor F-box protein, UNUSUAL FLORAL
31 ORGANS (UFO), but the molecular mechanism underlying this synergy has remained
32 unknown. Here, we show in transient assays and stable transgenic plants that the connection to
33 ubiquitination pathways suggested by the UFO F-box domain is mostly dispensable. Based on
34 biochemical and genome-wide studies, we establish that UFO instead acts by forming an active
35 transcriptional complex with LFY at newly discovered regulatory elements. Structural
36 characterization of the LFY-UFO-DNA complex by cryo-electron microscopy further
37 demonstrates that UFO performs this function by directly interacting with both LFY and DNA.
38 Finally, we propose that this complex might have a deep evolutionary origin, largely predating
39 flowering plants. This work reveals a novel mechanism of an F-box protein directly modulating
40 the DNA-binding specificity of a master TF.

41

42 **Main text**

43

44 The formation of flowers is key to the reproductive success of angiosperms. Flowers are made
45 of four types of organs (sepals, petals, stamens and carpels) arranged in concentric whorls. The
46 patterning of flower meristems requires the localized induction of the ABCE floral homeotic
47 genes that determine specific floral organ identities. In *Arabidopsis thaliana*, this
48 developmental step is largely controlled by the master transcription factor (TF) LEAFY (LFY)
49 that activates the ABCE genes^{1,2}. LFY directly activates the A class gene *APETALA1* (*API*)
50 uniformly in the early flower meristem^{3,4}, while activations of B and C genes are local and
51 require the activity of cofactors. For instance, LFY regulates the C class gene *AGAMOUS* (*AG*)

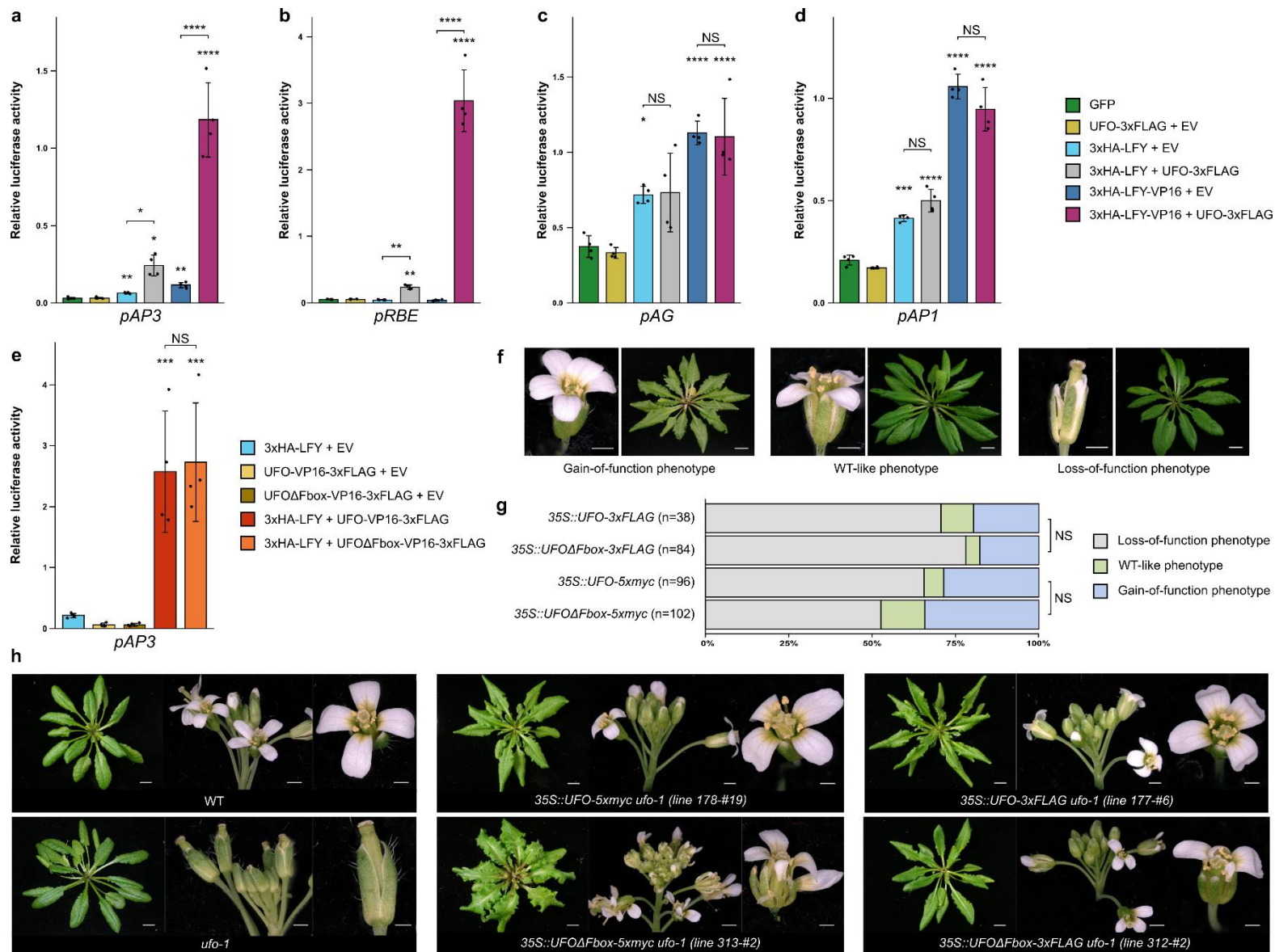
52 in conjunction with the TF WUSCHEL to specify third (stamen) and fourth whorl (carpel)
53 identities⁵. The activation of the B class gene *APETALA3* (*AP3*), necessary to specify the
54 identity of the second (petal) and third whorls of the flower, requires the combined activity of
55 LFY and the spatially-delineated cofactor UNUSUAL FLORAL ORGANS (UFO)⁶⁻⁸. In
56 Arabidopsis, the main function of LFY and UFO is to activate *AP3*⁹ but in numerous species
57 (such as rice, wheat, tomato or petunia), their joint role goes well beyond *B* genes activation
58 and is key to floral meristem and inflorescence development¹⁰⁻¹³.

59 At the molecular level, little is known on the nature of LFY-UFO synergy. Unlike most floral
60 regulators, *UFO* does not encode for a TF but for an F-box protein, one of the first to be
61 described in plants¹⁴⁻¹⁶. *UFO* is part of a SKP1-Cullin1-F-box (SCF) E3 ubiquitin ligase
62 complex through the interaction of its F-box domain with ARABIDOPSIS SKP1-LIKE (ASK)
63 proteins^{15,17}. In addition, its predicted C-terminal Kelch-type β -propeller domain physically
64 interacts with LFY DNA Binding Domain (DBD)¹⁸. As the control of TF activity through
65 proteolytic and non-proteolytic ubiquitination is a well-described mechanism¹⁹, it was
66 suggested that LFY is targeted for ubiquitination and possibly degradation by the SCF^{UFO}
67 complex. Other data showed that adding a repression or an activation domain to *UFO* changes
68 its activity and that *UFO* is recruited at the *AP3* promoter in a LFY-dependent manner, rather
69 suggesting a more direct role of *UFO* in gene regulation^{18,20}. However, direct evidence
70 explaining how *UFO* regulates a specific subset of LFY targets was still missing and the
71 molecular mechanism underlying LFY-UFO synergistic action remained elusive.

72 Here, we show that *UFO* connection to the SCF complex is largely dispensable for its activity
73 and that an important role of *UFO* is to form a transcriptional complex with LFY at genomic
74 sites devoid of canonical high-affinity LFY binding sites (LFYBS). Our study presents a unique
75 mechanism by which an F-box protein acts as an integral part of a transcriptional complex.

76
77

78 **Results**



79

80 **Fig. 1. UFO action is largely independent on its F-box domain.** a-e, Promoter activation in
 81 Arabidopsis protoplasts, with indicated effectors (right) and promoters (below each graph). EV
 82 = Empty Vector. Data are mean ± SD (n = 4 biological replicates). One-way ANOVA with
 83 Tukey's multiple comparisons test (c,d) or Welch's ANOVA with Games-Howell post-hoc test
 84 (a,b,e). Stars represent a significant statistical difference compared to GFP (a-d) or to 3xHA-
 85 LFY+EV (e), non-significant (NS) otherwise. Other comparisons are indicated with brackets.
 86 (NS: p > 0.05, *: p < 0.05, **: p < 0.01; ***: p < 0.001 and ****: p < 0.0001). f, Representative
 87 pictures of the different phenotypic classes obtained in the T1 population of indicated transgenic

88 plants (bars, 1 mm for flowers and 1 cm for rosettes). **g**, Distribution of T1 plants in phenotypic
89 classes as described in (f). The distribution of *35S::UFO* and *35S::UFOΔFbox* lines within
90 phenotypic classes is not significantly different (χ^2 tests, NS: $p > 0.05$). n = number of
91 independent lines. **h**, *ufo-1* complementation assay by the *35S::UFO* and *35S::UFOΔFbox*
92 transgenes. Rosette (scale bar, 1 cm), inflorescence (scale bar, 1 mm) and flower (scale bar, 0.5
93 mm) are shown.

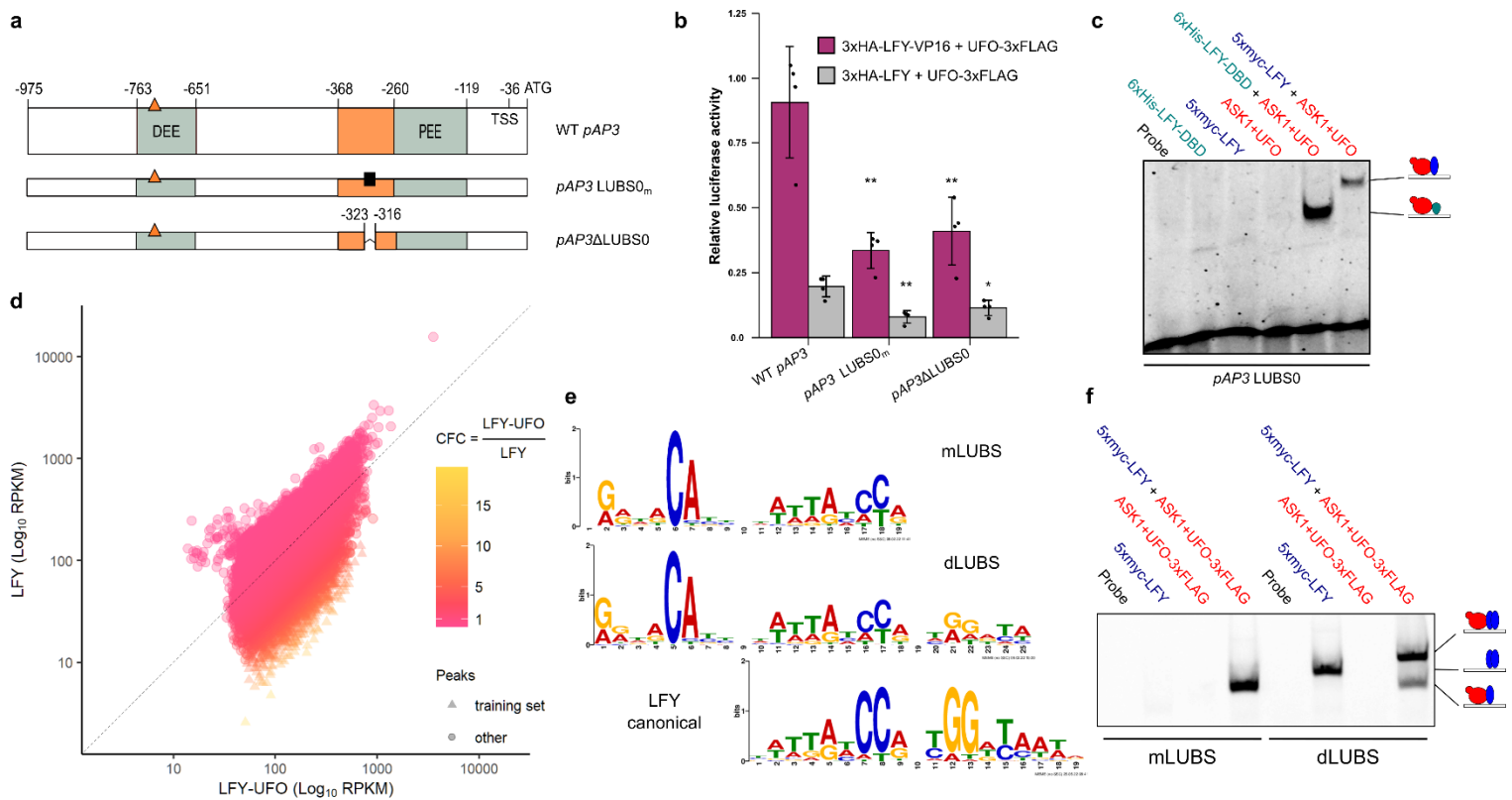
94

95 **UFO F-box domain is partially dispensable for its floral role.** A Dual Luciferase Reporter
96 Assay (DLRA) in Arabidopsis protoplasts was used to study floral promoter activation by LFY
97 and UFO. We used promoter versions known to allow full complementation of mutants or able
98 to recapitulate a WT expression pattern (see Methods). We found that the *AP3* promoter (*pAP3*)
99 was more strongly activated when LFY (or LFY-VP16, a fusion of LFY with the VP16
100 activation domain) was co-expressed with UFO (or UFO-VP16) than by either effector alone
101 (Fig 1a,e). Similar results were obtained with the promoter of *RABBIT EARS (RBE)*, another
102 UFO target (Fig. 1b)²². We also analyzed the promoters of *APETALA1 (pAPI)* and *AGAMOUS*
103 (*pAG*), two LFY targets regulated independently of UFO^{3,4,21} and that are required for organ
104 identity of the first and second (*API*) or third and fourth (*AG*) floral whorls. We found that their
105 activation by LFY and LFY-VP16 were insensitive to UFO (Fig. 1c,d). Thus, the protoplast
106 assay accurately reproduced several floral promoter activation patterns.

107 We next investigated the involvement of a SCF^{UFO}-dependent ubiquitination pathway in *pAP3*
108 activation by LFY-UFO. We found that, when co-expressed with LFY, N-terminally truncated
109 UFO versions lacking the F-box domain (*UFOΔFbox* and *UFOΔFbox-VP16*) activated *pAP3*
110 similarly to the full-length (FL) UFO (Fig. 1e). Thus, the connection of UFO to an SCF complex
111 appears dispensable for the *pAP3* activation in transient protoplast assays. The previously
112 reported inactivity of UFO with an internal deletion of its F-box likely reflects the poor folding

113 of this protein variant rather than the functional importance of the F-box domain (Extended
114 Data Fig. 1a-c)²⁰.

115 We also constitutively expressed tagged versions of UFO and UFO Δ Fbox in Arabidopsis.
116 Irrespective of the presence of the F-box, plants displaying a detectable UFO or UFO Δ Fbox
117 expression (Extended Data Fig. 1d) showed a typical UFO gain-of-function phenotype (Fig.
118 1f,g). In addition, both UFO versions complemented the strong *ufo-1* mutant and induced gain-
119 of-function phenotypes (Fig. 1h and Extended Data Fig. 1e,f)⁸. Still, minor defects (such as
120 some missing or misshapen petals and disorganized flowers) were specifically observed in the
121 absence of the F-box, suggesting that this conserved domain might be important for a subset of
122 UFO functions (Fig. 1h and Extended Data Fig. 1g). Overall, UFO and UFO Δ Fbox have a very
123 similar activity, showing that the role of the F-box domain is largely dispensable and that a
124 ubiquitination-independent mechanism determines the LFY-UFO synergy.



125

126 **Fig. 2. LFY and UFO together bind a new DNA motif.** **a**, WT *pAP3* with regulatory regions
 127 and *cis*-elements (top line). Coordinates are relative to *AP3* start codon. TSS: Transcription
 128 Start Site. Orange triangle represents canonical LFYBS. Detailed functional dissection of the
 129 107-bp region and the LUBS0 mutation are described in Extended Data Fig. 3. Other rows show
 130 the promoter versions used in **(b)**. **b**, *pAP3* activation in Arabidopsis protoplasts. Data are mean
 131 \pm SD ($n = 4$ biological replicates). One-way ANOVA with data from the same effector and
 132 Tukey's multiple comparisons tests. Stars represent a significant statistical difference compared
 133 to WT *pAP3* (*: $p < 0.05$, **: $p < 0.01$). **c**, EMSA with LUBS0 DNA probe and indicated
 134 proteins. Size Exclusion Chromatography coupled to Multi-Angle Laser Light Scattering
 135 established a mass of 102 ± 3.3 kDa for the ASK1-UFO-LFY-DBD-LUBS0 complex,
 136 consistent with a 1:1:1:1 stoichiometry (Extended Data Fig. 3e). Drawings represent the
 137 different complexes with FL LFY (blue), LFY-DBD (pale blue) and ASK1-UFO (red) on DNA.
 138 **d**, Comparison of peak coverage in LFY and LFY-UFO ampDAP-seq experiments, colored by

139 CFC. LFY-UFO-specific peaks used to build mLUBS and dLUBS motifs in (e) are triangle-
140 shaped. e, Logos for mLUBS, dLUBS and LFY binding site. The LFY logo was generated using
141 the 600 peaks with the strongest LFY ampDAP-seq signal. f, EMSA with mLUBS and dLUBS
142 highest score sequence DNA probes. Drawings represent the different complexes with LFY
143 (blue) and ASK1-UFO (red) on DNA.

144

145

146 **LFY and UFO form a transcriptional complex on a new DNA motif.** Protoplast assays
147 established that *AP3* and *RBE* promoter sequences contain the information that dictates their
148 specific activation by LFY-UFO. Several regulatory regions driving *AP3* regulation in early
149 floral meristem have been identified, including the Distal and the Proximal Early Elements
150 (DEE and PEE; Fig. 2a)^{23,24}. The DEE contains a predicted canonical LFY Binding Site
151 (LFYBS) but in protoplasts, like in plants²⁴, this site is not sufficient to explain *pAP3* activation
152 (Extended Data Fig. 2). By systematically testing *AP3* promoter variants in the transient assay,
153 we identified a 20-bp DNA element around the PEE important for LFY-UFO-dependent
154 activation but devoid of canonical LFYBS (Fig. 2b and Extended Data Fig. 3a-c). We
155 investigated the possibility that LFY and UFO form a complex on this DNA element using
156 electrophoretic mobility shift assay (EMSA). For this, we mixed either recombinant LFY DNA
157 Binding Domain (DBD, the LFY domain interacting with UFO)¹⁸ or *in vitro*-produced FL LFY,
158 with a reconstituted ASK1-UFO complex. None of the proteins bound the DNA probe alone,
159 but a shift was observed when LFY-DBD or FL LFY were mixed with ASK1-UFO (Fig. 2c).
160 Thus, a presumptive ASK1-UFO-LFY complex was formed on a *pAP3* DNA element (hereafter
161 named LFY-UFO Binding Site 0 or LUBS0) that each partner did not bind on its own. We did
162 note that UFO had a weak affinity for DNA as ASK1-UFO shifted the DNA probe when
163 performing EMSA with low competitor DNA concentrations (Extended Data Fig. 3d). Mutating

164 LUBS0 on various bases provided evidence that the formation of the complex is sequence-
165 specific and suggested a bipartite DNA motif (Extended Data Fig. 3f).

166 To identify all genome regions possibly targeted by the ASK1-UFO-LFY complex, we
167 performed ampDAP-seq (amplified DNA Affinity Purification sequencing) with a reconstituted
168 ASK1-UFO-LFY complex (Extended Data Fig. 4a,b). We identified numerous genomic regions
169 where LFY binding was strongly enhanced by the presence of ASK1-UFO. For each bound
170 region, we computed the ratio (named Coverage Fold Change or CFC) between the coverage
171 of peaks in the presence or absence of ASK1-UFO (Fig. 2d). Searches for enriched DNA motifs
172 in the 600 regions with the highest CFC (> 4.7) identified two bipartite motifs made of a 6-bp
173 RRNRCA (N=A/C/G/T, R=A/G) sequence, 4 bases of variable sequence and either a
174 monomeric or a dimeric site resembling canonical LFYBS but with more variability (Fig. 2e).
175 Consistent with the presence of a sequence resembling LFYBS, we found that *pAP3* activation
176 in protoplasts required the LFY amino-acid residues involved in binding to canonical LFYBS
177 (Extended Data Fig. 4c,d).

178 We named the identified motifs mLUBS and dLUBS for monomeric and dimeric LFY-UFO
179 Binding Sites, respectively (Fig. 2e). Since it is observed specifically with ASK1-UFO, the
180 RRNRCA element will be called UFO Recruiting Motif (URM). dLUBS and to a lesser extent
181 mLUBS Position Weight Matrices (PWM) outperformed LFY canonical PWM showing they
182 reliably predicted binding of ASK1-UFO-LFY (Extended Data Fig. 4e). The LFYBS present
183 within the LUBS of high CFC regions tended to have a lower predicted affinity than those
184 present in regions bound by LFY alone (Extended Data Fig. 4f), explaining why LFY binding
185 to those sequences occurs only with UFO and the URM. Remarkably, we also identified the
186 URM *de novo* from published LFY ChIP-seq data (Extended Data Fig. 4g)²⁵. Moreover, we
187 found that the LFY-ChIP-seq performed in inflorescences²⁵ correlates better with the ASK1-
188 UFO-LFY ampDAP-seq than with the LFY ampDAP-seq (Spearman rank correlation 0.481 vs

189 0.338 for the first 1000 ChIP-seq peaks), strongly suggesting that many regions are bound *in*
190 *vivo* by UFO (see examples of such regions in Extended Data Fig. 7b,c).

191 AmpDAP-seq findings were validated by EMSA with DNA probes corresponding to optimal
192 mLUBS and dLUBS motifs (Fig. 2f and Extended Data Fig. 4h). We observed a complex of
193 slower mobility with dLUBS as compared to mLUBS, consistent with the presence of two LFY
194 molecules on dLUBS. ASK1-UFO also supershifted LFY bound to canonical LFYBS from
195 *pAP1* and *pAP3* DEE (Extended Data Fig. 4i), sometimes (but not systematically) increasing
196 apparent LFY binding.

197

198

199

200

201

202

203

204

205

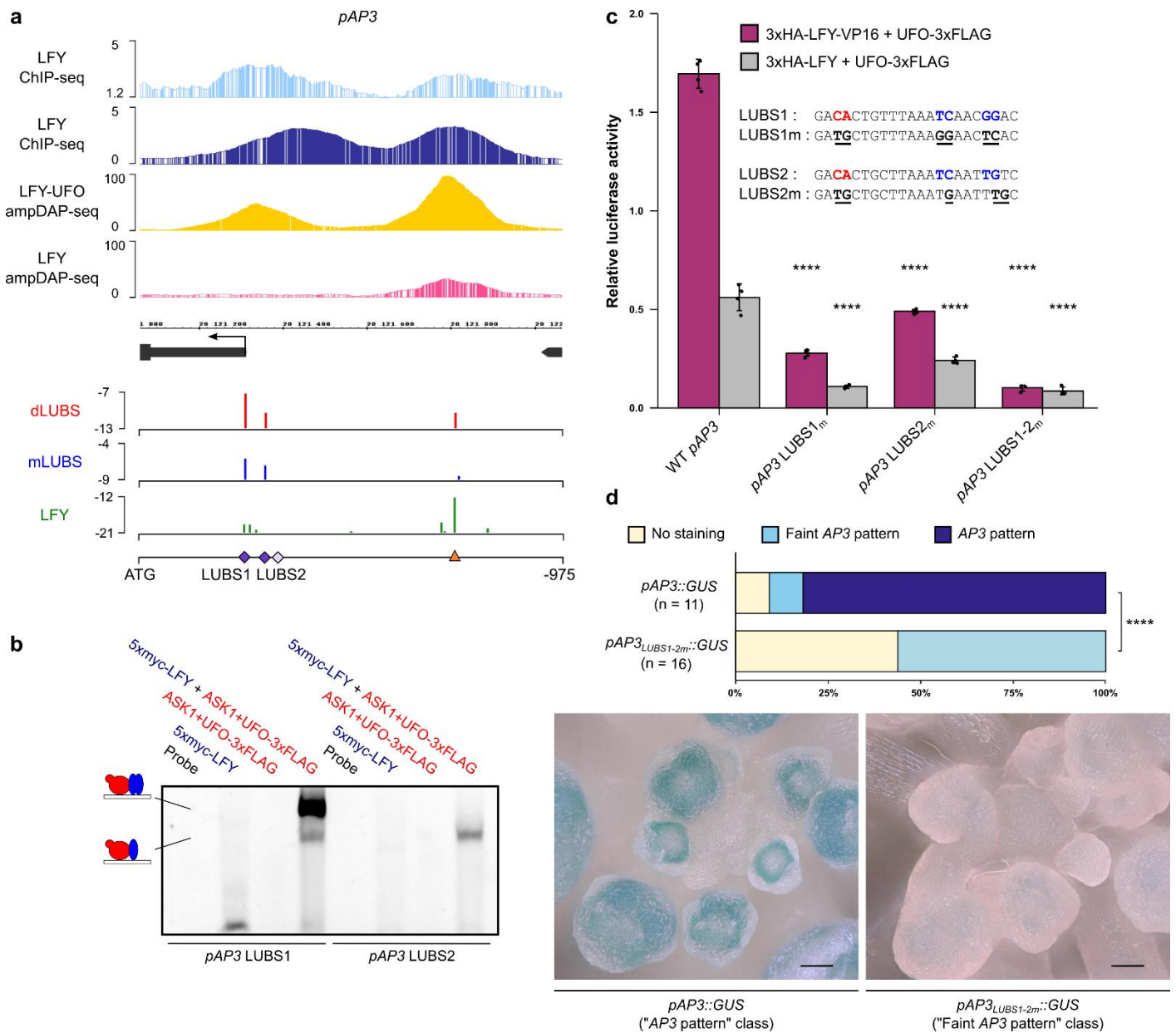
206

207

208

209

210



211

212 **Fig. 3. Functional validation of LUBS.** **a**, Integrated Genome Browser (IGB) view of *pAP3*
 213 showing LFY ChIP-seq in inflorescences (light blue)²⁵ or seedlings (dark blue)²⁶, LFY-UFO
 214 ampDAP-seq (yellow) and LFY ampDAP-seq (pink)²⁷, y-axis indicates read number range
 215 (top). Identification of LUBS in *pAP3* (bottom). Predicted binding sites using dLUBS and
 216 mLUBS models and LFY PWM, y-axis represents score values. LUBS1 and LUBS2 are
 217 indicated with purple squares, canonical LFYBS as an orange triangle. LUBS0 (light purple
 218 square) is not visible because of its low score. **b**, EMSA with *pAP3* LUBS probes. Drawings

219 represent the different complexes involving LFY (blue) and ASK1-UFO (red) on DNA. **c**,
220 *pAP3* activation in Arabidopsis protoplasts. Effect of mutations (underlined) in URM (red) and
221 LFYBS (blue) bases of *pAP3* LUBS were assayed. Data are mean \pm SD (n = 4 biological
222 replicates). One-way ANOVA performed with data from the same effector and with Games-
223 Howell post-hoc test. Stars represent a statistical difference compared to WT promoter (****:
224 $p < 0.0001$). **d**, *In vivo* analysis of *pAP3::GUS* fusions. Percentage of transgenic lines with an
225 *AP3* pattern, a faint *AP3* pattern or absence of staining (top). Pattern distributions are different
226 between the two constructs (χ^2 test, ****: $p < 0.0001$). n = number of independent lines.
227 Representative pictures of plants with an *AP3* pattern (bottom left) and a faint *AP3* pattern
228 (bottom right, scale bar, 50 μ m). Note the staining in the ring corresponding to 2nd and 3rd whorl
229 primordia in the left picture.

230

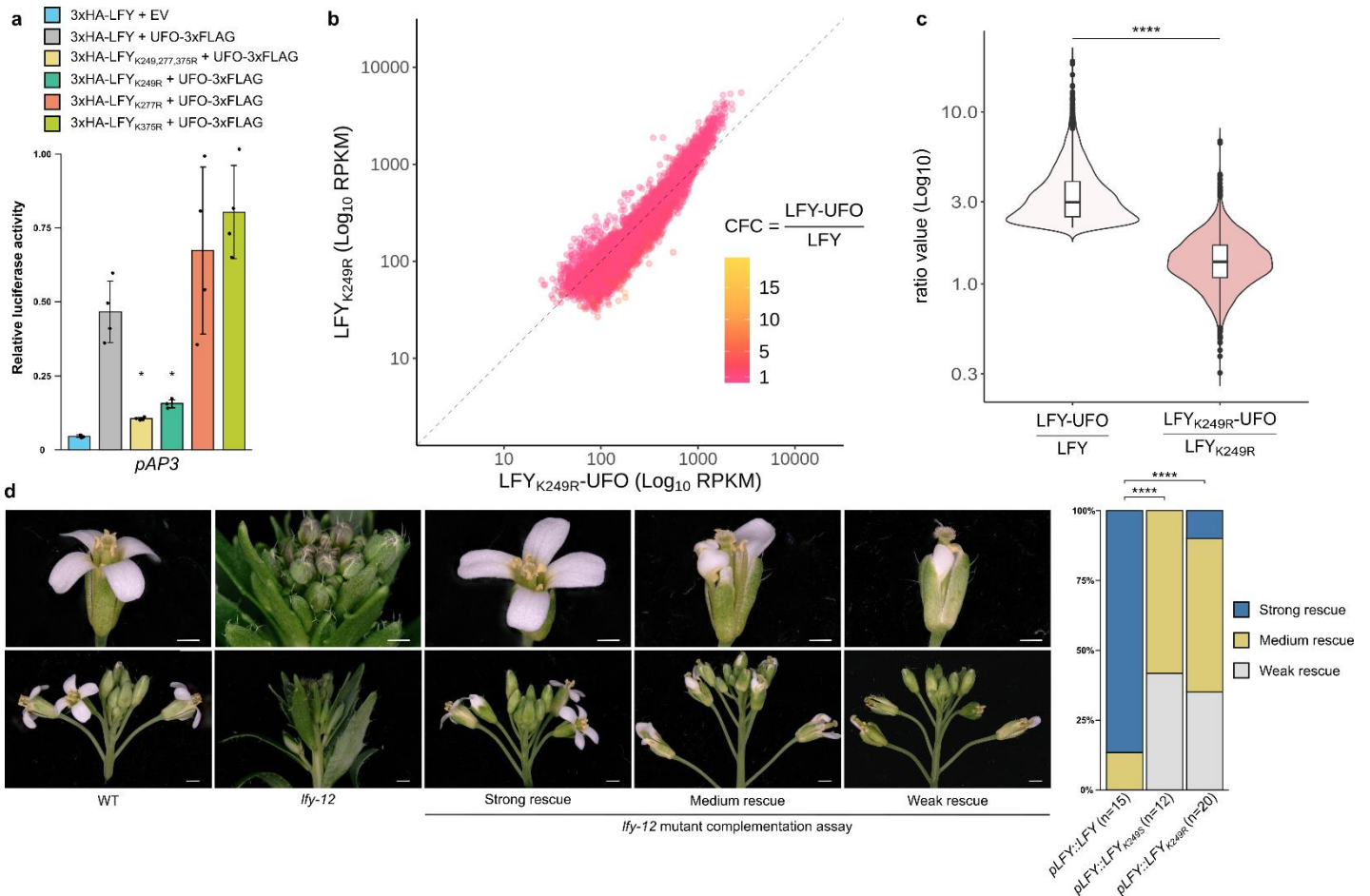
231

232 **LUBS are functional regulatory elements.** Examination of *pAP3* genomic region in ASK1-
233 UFO-LFY ampDAP-seq revealed a peak that is absent in the experiment performed with LFY
234 alone (Fig. 3a). This peak is roughly located on the PEE and is consistent with LFY CHIP-seq
235 peaks^{25,26}. We searched for LUBS under this peak and, to our surprise, we identified several
236 sites predicted to be better than LUBS0 (Fig. 3a). In EMSA, the two highest score sites, LUBS1
237 and LUBS2, were specifically bound by LFY in the presence of ASK1-UFO (Fig. 3b and
238 Extended Data Fig. 5a). EMSAs performed with a LFY mutant version affected in its ability to
239 dimerize further confirmed the stoichiometry of LFY-UFO complexes on LUBS1 and LUBS2
240 (Extended Data Fig. 5b). A similar binding was also observed when combining LFY and
241 UFO Δ Fbox (Extended Data Fig. 5c,d), consistent with the F-box being facultative for LFY-
242 UFO transcriptional activity (Fig. 1). In the protoplast assay, mutating LUBS1 or LUBS2 (or
243 both) significantly reduced *pAP3* activation (Fig. 3c) with a stronger effect of the LUBS1

244 mutation. Specifically mutating the URM of *pAP3* LUBS1 and LUBS2, that abolished LFY-
245 UFO binding on individual sites in EMSA (Extended Data Fig. 5e), also reduced *pAP3*
246 activation albeit less effectively than mutating the whole LUBS (Extended Data Fig. 5f).
247 Finally, the previously described *pAP3::GUS* staining pattern in the second and third whorls of
248 Arabidopsis early floral meristems was severely reduced when LUBS1 and LUBS2 were
249 mutated, demonstrating the importance of these sites *in vivo* (Fig. 3d and Extended Data Fig.
250 5g). Similarly, the *RBE* promoter contains an ASK1-UFO-LFY ampDAP-seq peak that is
251 absent with LFY alone (Extended Data Fig. 6a), and the functional importance of the single
252 LUBS identified under this peak was confirmed using EMSA, transient assay in protoplasts and
253 stable reporter constructs in plants (Extended Data Fig. 6b-e).

254 In addition to *AP3* and *RBE*, LFY and UFO together likely regulate many other genes in
255 Arabidopsis. To identify such potential LFY-UFO targets, we established a list of genes bound
256 (in ampDAP and CHIP) and regulated by LFY-UFO (Extended Data Fig. 7a). This procedure
257 identified the other B gene *PISTILLATA*, previously proposed as a LFY-UFO target but through
258 an unknown regulatory element that the LUBS model precisely localized (Extended Data Fig.
259 7b). We also found floral regulators such as *SQUAMOSA PROMOTER BINDING PROTEIN-*
260 *LIKE 5* and *FD* as well as novel candidates likely regulated by LFY and UFO (Extended Data
261 Fig. 7a,c).

262



263

264 **Fig. 4. The LFY K249R mutation disrupts the LFY-UFO synergy.** **a**, *pAP3* activation in
 265 Arabidopsis protoplasts. Data are mean \pm SD (n = 4 biological replicates). Welch's ANOVA
 266 with Games-Howell post-hoc test. Stars indicate a statistical difference compared to 3xHA-
 267 LFY+UFO-3xFLAG. (NS: $p > 0.05$,*: $p < 0.05$). **b**, Comparison of peak coverage in LFY_{K249R}-
 268 UFO (x-axis) and LFY_{K249R} (y-axis) ampDAP-seq experiments, colored by peak coverage ratio
 269 (CFC) as in Fig. 2d. Note that, in contrast to Fig. 2d, the LFY-UFO-specific regions are mostly
 270 absent. **c**, Distribution of coverage ratios for LFY and LFY_{K249R} for LFY-UFO-specific regions
 271 (20% highest CFC; n = 3843 genomic regions). Wilcoxon's rank sum test (***: $p < 0.0001$).
 272 Median (solid line), interquartile range (box edges), $\pm 1.5 \times$ interquartile range (whiskers) and
 273 outliers (black dots) are shown. **d**, *lfy-12* mutant complementation assay. Pictures of WT, *lfy*-
 274 *12* mutant and of representative plants of the different phenotypic complementation classes

275 (left, scale bar 1 mm for top pictures and 1 cm for bottom pictures). Distribution of the different
276 lines within phenotypic complementation classes (right). Plants complemented with LFY_{K249R}
277 and LFY_{K249S} show different complementation patterns compared to plants complemented with
278 LFY (χ^2 tests, ****: $p < 0.0001$). n = number of independent lines.

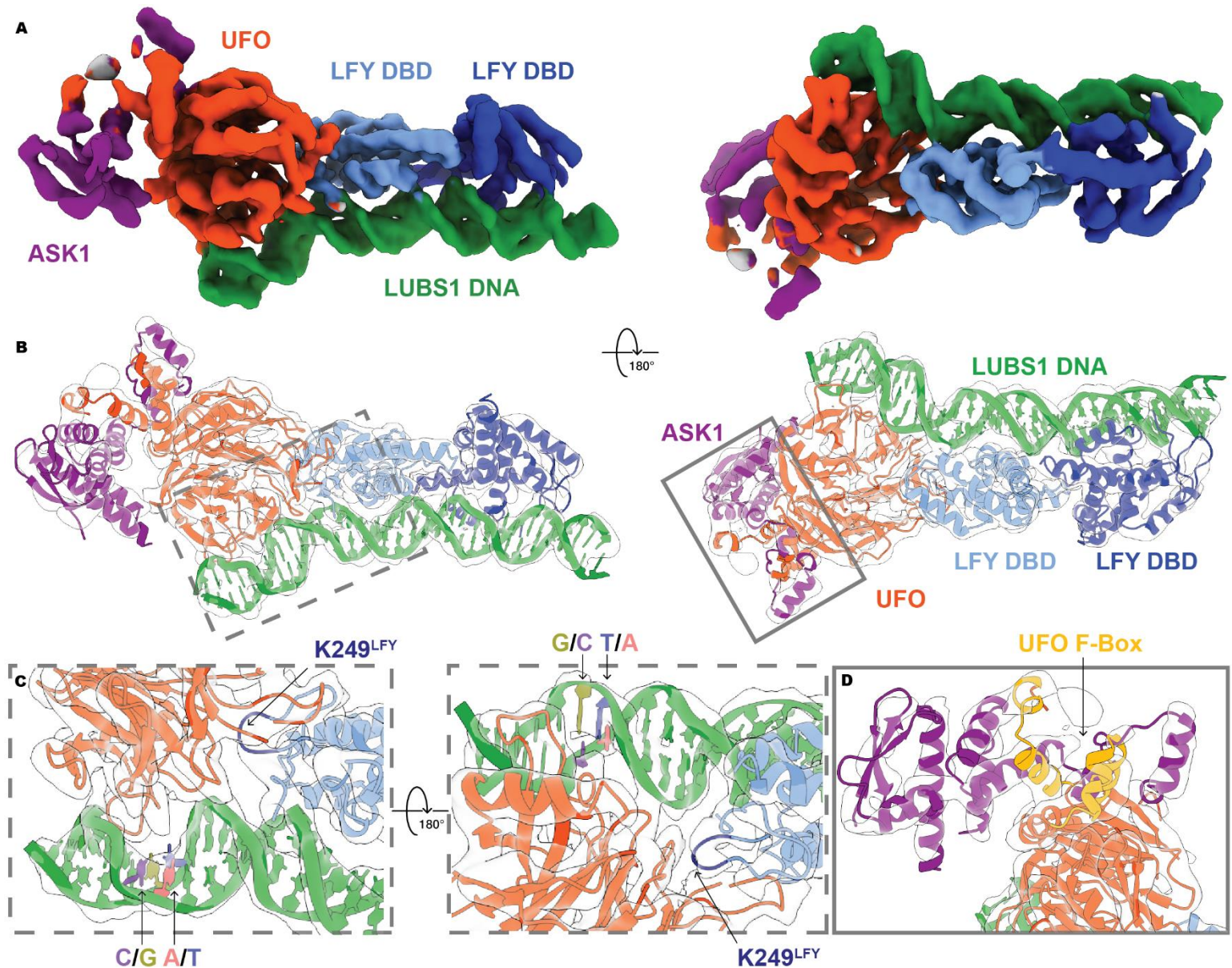
279

280

281 **The LFY K249R mutation specifically affects UFO-dependent LFY functions.** In
282 Arabidopsis, LFY performs UFO-dependent and independent functions³, and we wondered
283 whether they could be uncoupled by introducing specific mutations in LFY. As we were
284 initially looking for LFY ubiquitination mutants, we mutated exposed lysines of LFY-DBD into
285 arginines, and tested the effect of such mutations on LFY-UFO-dependent *pAP3* activation in
286 protoplasts. We found one mutation (LFY K249R; Extended Data Fig. 8a) that strongly reduced
287 *pAP3* activation by LFY-UFO (Fig. 4a) or LFY-VP16-UFO (Extended Data Fig. 8b) without
288 affecting the UFO-independent *pAG* activation (Extended Data Fig. 8c) or the LFY-UFO
289 interaction (Extended Data Fig. 8d). AmpDAP-seq experiments showed that the LFY K249R
290 mutation specifically impaired the binding of LFY-UFO but not that of LFY alone (Fig. 4b,c
291 and Extended Data Fig. 8e-i), revealing that K249 plays a key role in LFY-UFO interaction
292 with the LUBS DNA.

293 The importance of LFY K249 for UFO-dependent LFY functions was also confirmed using
294 complementation assay of the Arabidopsis *lfy-12* null mutant²⁸. *lfy-12* plants expressing
295 LFY_{K249R} or LFY_{K249S} under the control of *LFY* promoter developed flowers with normal sepals
296 and carpels but with defective third and more importantly second whorl organs, resulting in
297 flowers similar to those observed in weak *ufo* mutants (Fig. 4d). When expressed under the
298 constitutive 35S promoter, LFY_{K249R} triggered ectopic flower formation and early flowering

299 like WT LFY (Extended Data Fig. 8j), consistent with these LFY functions being independent
300 of UFO and thus not affected by the K249R mutation²⁹.



301

302 **Fig. 5. Structural characterization of the ASK1-UFO-LFY-DNA complex.** **a**, Cryo-EM
 303 density map of the ASK1-UFO-LFY-DBD-LUBS1 complex under two angles, colored with
 304 regard to the underlying macromolecule (green: LUBS1 DNA; pale and dark blue: LFY-DBD;
 305 red: UFO; purple: ASK1). **b**, The same views of the cryo-EM density map in transparent gray
 306 with fitted structures of LFY-DBD dimer, UFO, ASK1 and LUBS1 DNA. Same colors as in
 307 **(a)**. The frames roughly indicate the regions shown in **(c)** and **(d)**. **c**, Zoom on the UFO-DNA
 308 contact region (left) and on the LFY-UFO interface (right). Only the high-information CA of

309 the URM and its complement is highlighted by filled coloring the rings for each base (red for
310 A, blue for T, pale green for G and purple for C). The LFY-DBD loop containing the K249
311 residue is highlighted in dark blue. **d**, Zoom on the ASK1-UFO interface, with the UFO F-box
312 highlighted in gold.

313

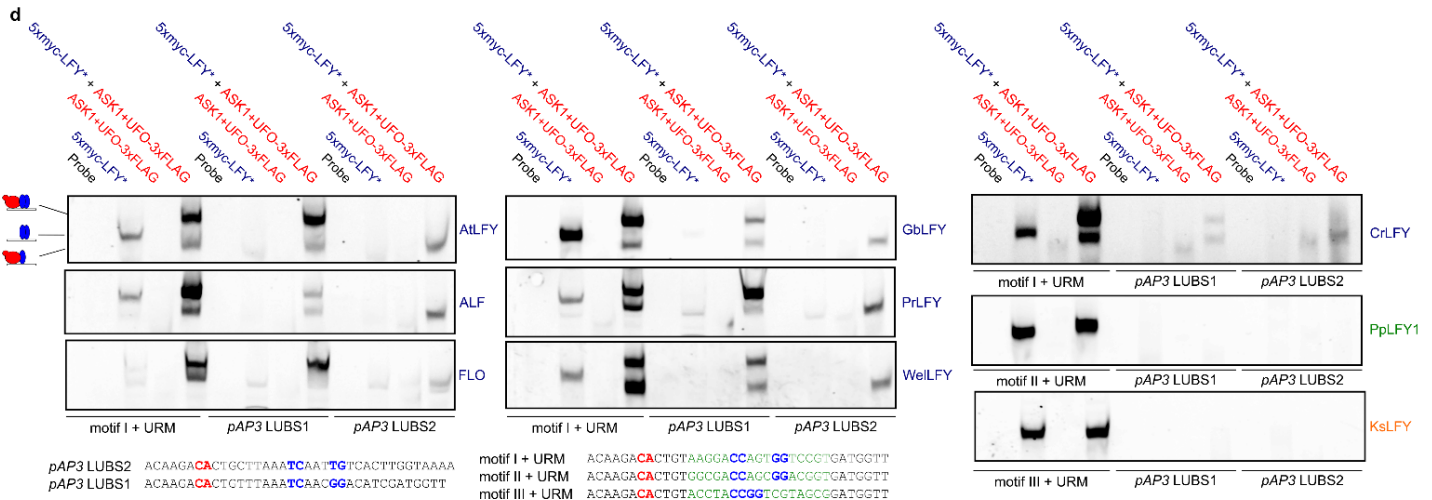
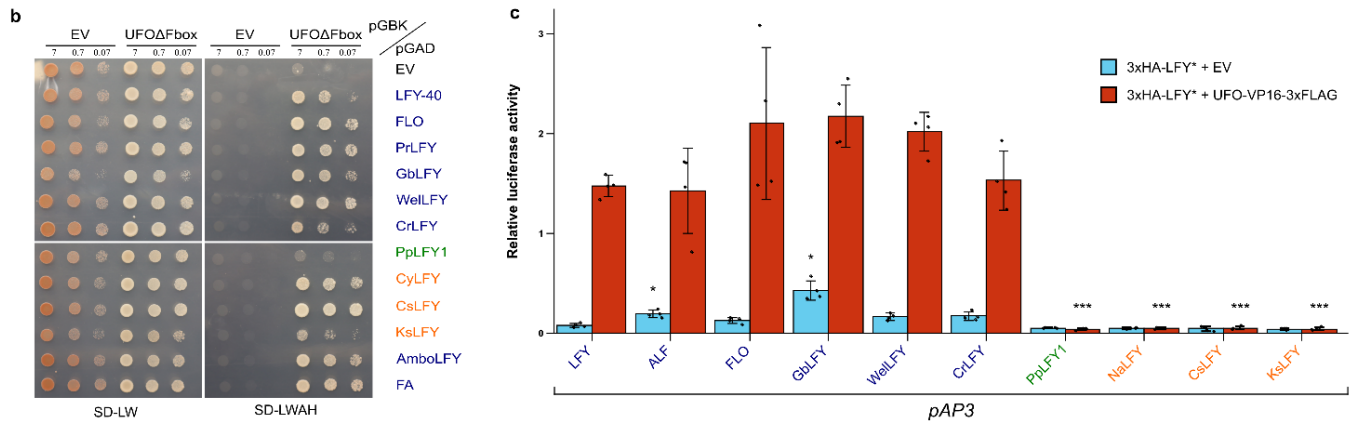
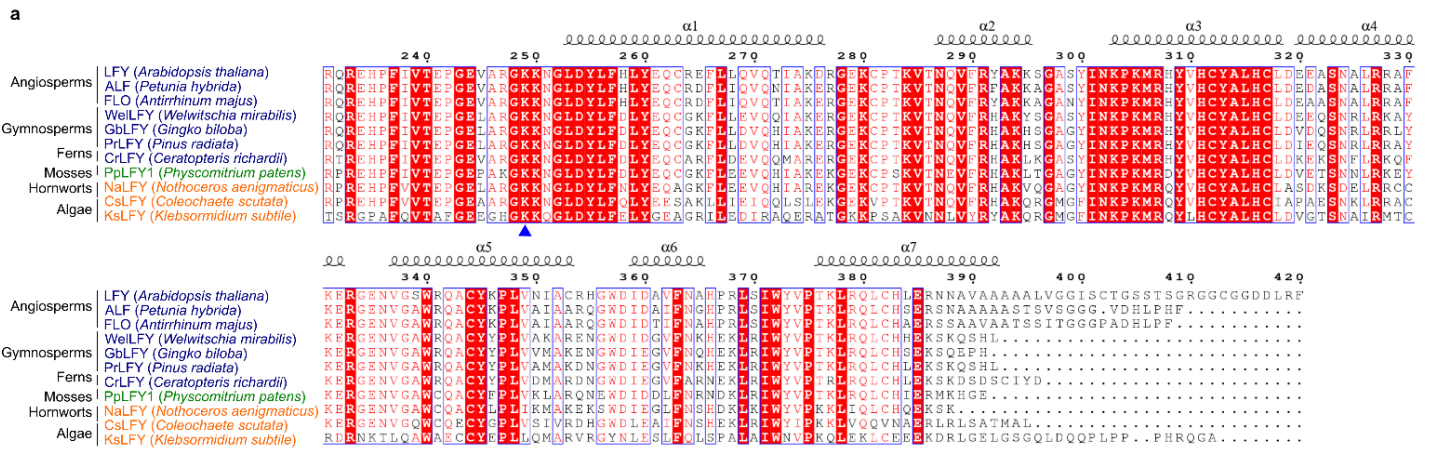
314

315 **Structural characterization of the ASK1-UFO-LFY-DNA complex.** In order to understand
316 how the LFY-UFO complex recognizes its cognate DNA binding site and how the K249
317 mutation impedes this interaction, we purified the ASK1-UFO-LFY-DBD-LUBS1 complex
318 and we structurally characterized it using cryo-electron microscopy (Fig. 5a and Extended Data
319 Fig. 9a-d). A structure at a 4.27 Å resolution was obtained (Extended Data Fig. 9g-i) into which
320 were fit the AlphaFold2 predicted structure for UFO and ASK1, and the LFY-DBD dimer/DNA
321 crystallographic structure³⁰ (PDB, 2VY1; Fig. 5b and Extended Data Fig. 9e,f). Due to the
322 modest resolution, specific interacting amino acids could not be unambiguously identified.
323 However, the major protein-protein and protein-DNA interaction surfaces were clearly
324 identifiable.

325 The structure revealed that UFO directly contacts the DNA in the major groove around the
326 URM (Fig. 5c). This binding likely involves basic residues present on loops projecting from
327 the UFO Kelch-type β -propeller and results in a bend of roughly 30 degrees in the DNA double
328 helix (Extended Data Fig. 9f). The structure also shows an interface between UFO and one
329 LFY-DBD monomer (Fig. 5c). The LFY-DBD loop containing the K249 residue lies in this
330 interface and likely interacts with one of the DNA-binding loops of UFO, consistent with the
331 key role of LFY K249 in the ternary complex formation. As expected, ASK1 interacts with
332 UFO F-box domain¹⁵ (Fig. 5D).

333 These data show how a β -propeller protein is able to modify the specificity of a TF, and offer a
334 structural explanation on how LFY and UFO synergistically recognize a novel DNA element
335 via direct interactions by both proteins with the DNA.

336



337

338 **Fig. 6. LFY-UFO interaction is conserved beyond angiosperm species. a**, Alignment of LFY

339 DBDs. Amino acid numbering and secondary structure annotation are based on LFY from *A.*

340 *thaliana*. LFY K249 residue is indicated with a blue triangle. DNA binding specificities are

341 color-coded, type I (blue), II (green) and III (orange). FLO = FLORICAULA; ALF =

342 ABERRANT LEAF AND FLOWER. **b**, Interaction between LFY orthologs and AtUFOΔFbox

343 in Y2H. LFY orthologs are described in (a) except CyLFY (*Cylindrocystis sp.*), AmboLFY

344 (*Amborella trichopoda*) and FA (FALSIFLORA; *Solanum lycopersicum*). See Extended Data
345 Fig. 4d for legends. **c**, *pAP3* activation measured by DLRA in Arabidopsis protoplasts. EV =
346 Empty Vector. 3xHA-LFY* refers to the different LFY orthologs indicated under the x-axis.
347 Data represent averages of independent biological replicates and are presented as mean \pm SD,
348 each dot representing one biological replicate (n = 4). Welch's ANOVA with Games-Howell
349 post-hoc test. One-way ANOVA was performed with data from the same effector (described in
350 the legend), and stars represent a statistical difference compared to AtLFY, NS otherwise. (NS:
351 $p > 0.05$, *: $p < 0.05$, **: $p < 0.01$; ***: $p < 0.001$). **d**, EMSA with indicated DNA probes
352 (bottom). URM and LFYBS bases are depicted in red and blue, respectively. *pAP3* LUBS1
353 sequence was modified to insert the perfect sequence of motif I, II or III³¹ (depicted in green):
354 these DNA probes were used as positive controls for binding of LFYs alone and LFY-UFO
355 complex formation. 5xmyc-LFY* refers to the different LFY orthologs indicated next to each
356 EMSA and described in (a).

357

358

359 **The LFY-UFO complex might have a deep evolutionary origin**

360 As genetic and physical LFY-UFO interactions have been described in diverse angiosperms,
361 we wondered whether the mechanism unraveled for Arabidopsis proteins could also apply to
362 LFY from other species, including non-angiosperm ones. We selected LFY orthologous
363 proteins from several species and with different DNA binding specificities (Fig. 6a). Indeed,
364 through evolution, LFY specificity evolved with three major DNA binding specificities³¹. Type
365 I specificity is the one described in Arabidopsis and valid for other angiosperms, gymnosperms,
366 ferns and the moss *Marchantia polymorpha*, with two half-sites separated by a 3-bp spacer (Fig.
367 2e). LFY from the moss *Physcomitrium patens* have a type II specificity with specific half-sites
368 (different from type I half-sites) also separated by a 3-bp spacer. Finally, type III specificity is
369 found for LFY from algae and corresponds to a type II motif without the spacer. Because

370 functional UFO homologs have not been identified outside angiosperms, we used Arabidopsis
371 UFO (AtUFO) in all the following experiments.
372 We tested the interaction of various LFY orthologs with AtUFO in Y2H (Fig. 6b), in DLRA in
373 protoplasts with Arabidopsis *pAP3* (Fig. 6c) and in EMSA (Fig. 6d). In Y2H, all LFYs except
374 LFY from *P. patens* (Type II) interact with AtUFO (Fig. 6b). However only Type I LFY from
375 angiosperms, gymnosperms and ferns form a complex on *pAP3* LUBS and activate *pAP3* in the
376 protoplast assay (Fig. 6c,d). These results suggest that the ability of LFY and UFO to act
377 together by forming a complex is ancient, largely predating the origin of angiosperms. We
378 obtained no evidence that type II and III LFY (from moss and algae) could form a complex
379 with AtUFO on LUBS1 and LUBS2. A detailed and more trustworthy history of the LFY-UFO
380 interaction will await further analyses, notably with the identification of UFO orthologs from
381 non-angiosperm genomes.

382

383 **Discussion**

384

385 LFY was long known to interact with UFO to control flower and inflorescence development in
386 numerous angiosperm species. However, the molecular nature of their synergistic action had
387 remained unknown. As UFO encodes an F-box protein taking part in an SCF complex^{17,32,33}, it
388 was thought to target proteins for a SCF^{UFO}-dependent ubiquitination and possible degradation.
389 LFY was an obvious target candidate but clear evidence of LFY ubiquitination was missing
390^{12,18}. The results we present here suggest that the F-box domain, required for ubiquitination, is
391 dispensable for most UFO-dependent LFY activity. Nevertheless, the high conservation level
392 of UFO F-box sequence in angiosperms, together with slight differences in UFO activity when
393 the F-box is deleted suggest that this domain might still be needed for some elusive facets of
394 UFO function. UFO may work redundantly with other F-box proteins in ubiquitination

395 pathways like with the F-box protein HAWAIIAN SKIRT identified in a genetic screen as an
396 enhancer of *ufo* mutant phenotype³⁴. It is thus possible that UFO acts as a moonlighting
397 protein³⁵ with functions in both transcription and ubiquitination, and these two activities could
398 be related or independent.

399 The molecular mechanism we discovered here is consistent with most published data on *AP3*
400 and *PI* regulation^{18,23,36,37}. However, a detailed understanding of the expression pattern of *AP3*
401 and *RBE* will require further work on other *cis* and *trans*- elements. Why *AP3* is not transcribed
402 in floral stage 0-1 despite the expression of LFY and UFO is unclear²⁰. It could be because
403 SUPPRESSOR OF OVEREXPRESSION OF CO 1 (SOC1), AGAMOUS-LIKE 24 (AGL24)
404 and SHORT VEGETATIVE PHASE (SVP) act as early *AP3* repressors as *AP3* mRNA is
405 detected in the floral anlage in a *soc1 svp agl24* mutant^{38,39}. Another explanation could be that
406 *AP3* expression requires the *SEPALLATA3* activator⁴⁰. Why *pAP3* is not activated by LFY (or
407 LFY-VP16) alone through the canonical LFYBS is also an open question.

408 Our work unraveled an unsuspected function unrelated to ubiquitination for UFO: it forms a
409 transcriptional complex with LFY at regulatory sites that are different from the canonical sites
410 bound by a LFY homodimer. UFO was previously proposed to act in transcription, but in the
411 absence of direct evidence that a LFY-UFO complex forms on novel binding sites, it was
412 difficult to understand how UFO controls only a subset of LFY targets. These novel regulatory
413 sites (mLUBS and dLUBS) are made of a low-affinity or half LFYBS (poorly or not bound by
414 LFY alone) and a motif located at a fixed distance from it and responsible for UFO recruitment.
415 The formation of such a sequence-specific complex is explained at the structural level by the
416 capacity of UFO to interact with both LFY and DNA. The poor ability of UFO to bind DNA
417 alone explains its complete dependence on LFY to perform its transcriptional functions *in*
418 *planta*^{6,20}. Thus, depending on *cis*-elements present in regulatory regions, LFY either binds

419 DNA as a homodimer or requires UFO to form a ternary complex. Mutation of the LFY K249
420 residue allows uncoupling these two types of binding by specifically disrupting the formation
421 of the LFY-UFO-DNA complex. The position of this residue in the 3D structure at the interface
422 between LFY, UFO and DNA is consistent with the key role of this residue in the complex
423 formation. It is possible that replacing K249 with a bulkier R residue displaces the UFO loops
424 involved in DNA binding without affecting the LFY-UFO interaction. Obtaining a higher-
425 resolution structure will help to understand precisely the interactions occurring in this complex.
426 Although it might be a common regulatory mechanism, only few cases where non-TF proteins
427 modify TF DNA binding specificity have been described so far (for example Met4 and Met28
428 modifying the binding of TF Cbf1 in yeast⁴¹, or the herpes simplex virus transcriptional
429 activator VP16 changing specificity of the Oct-1/HCF-1 complex⁴²). None of these examples
430 involves an F-box protein or a Kelch-type β -propeller protein and neither of them has been
431 characterized at the structural level. TF DNA binding specificity modification by non-TF
432 proteins offers additional possibilities for a combinatorial control of gene expression and
433 explains how a master regulator such as LFY accesses novel *cis*-elements to perform different
434 functions in distinct territories.

435 Since LFY and UFO play key roles together in numerous plants species (including ornamental,
436 crops and model plants), our findings expand the molecular understanding of flower and
437 inflorescence development in a large variety of angiosperms. Because the LFY-UFO synergy
438 is observed with LFY orthologs from gymnosperms and ferns as well, we speculate that this
439 complex largely predated the origin of flowers and could have been coopted for flower
440 development from a yet unknown ancestral role.

441

442 **Acknowledgements**

443

444 We thank AM. Boisson for preparing suspension cells, X. Lai for ampDAP-seq libraries and
445 technical assistance and R. Koes for sharing data and materials. We gratefully acknowledge C.
446 Maronedze, G. Vachon, M. Le Masson, C. Berthollet, B. Orlando Marchesano and J.
447 Bourenane-Vieira for help with experiments. We thank G. Vert, U. Dolde and R. Dumas for
448 discussion. The electron microscopy facility is supported by the Rhône-Alpes Region, the FRM,
449 the FEDER and the GIS-IBISA. This work used the platforms of the Grenoble Instruct-ERIC
450 center (ISBG; UAR 3518 CNRS-CEA-UGA-EMBL) within the Grenoble Partnership for
451 Structural Biology (PSB), supported by FRISBI (ANR-10-INBS-0005-02). We thank Caroline
452 Mas for assistance and access to the biophysical platform. This work was supported by the
453 GRAL Labex financed within the University Grenoble Alpes graduate school (Ecoles
454 Universitaires de Recherche) CBH-EUR-GS (ANR-17-EURE-0003), the CEA (PhD fellowship
455 to PR) and the ANR-17-CE20-0014-01 Ubiflor project to FP.

456

457 **Author contributions**

458

459 FP and PR designed the project. PR performed the plant experiments helped by GT. PR and ET
460 performed the biochemical experiments helped by HC for evolutionary analyses. LT performed
461 the bioinformatics analyses helped by JL and RBM. EZ and GS performed cryo-EM
462 experiments and MN, EZ, CZ and GS analyzed the data. PR and LT assembled the figures. PR
463 and FP wrote the paper with contributions from LT and CZ.

464

465 **Competing interests**

466

467 We declare no competing interests.

468

469 **Methods**

470

471 **Arabidopsis growth.** All mutants and transgenic lines are in the *A. thaliana* Columbia-0
472 accession. Seeds were sown on soil, stratified 3 days at 4 °C, and then grown at 22°C under
473 long-day conditions (16 h light). Transgenic plants were obtained with *Agrobacterium*
474 *tumefaciens* C58C1 pMP90 using the floral dip method. Transformants were identified using
475 GFP or Basta selection.

476

477 **Arabidopsis cell suspension culture.** *Arabidopsis thaliana* (ecotype Columbia-0) cells in
478 suspension cultures were grown under continuous light (90 μmol of photons $\text{m}^{-2} \text{s}^{-1}$) at 21°C
479 with shaking at 135 rpm in Murashige and Skoog (MS) medium supplemented with 30 g/L
480 sucrose and 2 mg/L 2,4-dichlorophenoxyacetic acid (2,4D), pH 5.5. Suspension cells were
481 subcultured every week with a 5-fold dilution. Suspension cells at 4 or 5 days following
482 subculture were used for protoplast preparation.

483

484 **Cloning.** DNA fragments were amplified by PCR with Phusion high fidelity polymerase
485 (NEB). Plasmids were all obtained by Gibson Assembly (GA) with either PCR-amplified or
486 restriction enzyme-digested backbone vectors. We used the 420 aa LFY version. For site-
487 directed mutagenesis, primers containing the desired mutations were used for GA mutagenesis.
488 Plasmids were obtained using DH5 α bacteria and were all verified by Sanger sequencing. A list
489 of plasmids and cloning procedures is provided in Supplementary Data 1. Oligonucleotide
490 sequences are listed in Supplementary Data 2.

491

492 **Yeast-two-hybrid.** Coding sequences were cloned in pGADT7-AD or pGBKT7 vectors
493 (Clontech) by GA. Y187 and AH109 yeast strains (Clontech) were transformed with pGADT7-

494 AD or pGBKT7 vectors and selected on plates lacking Leucine (SD-L) or Tryptophan (SD -
495 W), respectively (MP Biomedicals). After mating, yeasts were restreaked on plates lacking
496 Leucin and Tryptophan (SD -L-W) for 2 days. Yeasts were then resuspended in sterile water
497 and OD_{600nm} was adjusted to indicated values for all constructions; two ten-fold dilutions were
498 performed, and 6 µL drops were done on SD -L-W or SD -L-W-A-H (lacking leucine,
499 tryptophan, histidine and adenine) plates. Yeasts were grown at 28°C and pictures were taken
500 at indicated times.

501

502 **Dual Luciferase Reporter Assay (DLRA) in Arabidopsis protoplasts.** Effector plasmids
503 with a 3xHA tag were obtained by cloning indicated genes in the modified pRT104 vector
504 containing a 3xHA N-terminal tag (pRT104-3xHA)⁴³. The pRT104 empty plasmid was
505 reengineered to insert a 3xFLAG C-terminal tag. For reporter plasmids, indicated promoter
506 fragments were cloned upstream a Firefly Luciferase gene in pBB174⁴⁴. We used a 975-bp
507 *pAP3* fragment and a 2-kb *pRBE* promoter fragment upstream of the ATG, known to induce a
508 WT pattern in plant^{23,45}. *pAG* corresponds to *AG* second intron fused to a minimal 35S promoter,
509 known to induce a WT pattern in plant²¹. For *pAPI*, we used a 600-bp fragment upstream of
510 the ATG. This version is sufficient to give a WT pattern in plant⁴⁶, and the use of longer
511 promoter versions induced a very high background noise in protoplasts. The pRLC reference
512 plasmid contains Renilla Luciferase sequence under the control of the 35S promoter. Plasmids
513 were obtained in large amounts using NucleoBond Xtra Maxi Plus kit (Macherey-Nagel).
514 Protoplasts were prepared from Arabidopsis Col-0 cell suspension and transformed following
515 the procedure described by Iwata et al.⁴⁷. Cell wall was digested using Onuzuka R-10 cellulase
516 and macerozyme R-10 (Yakult Pharmaceutical). Digested cells were passed through two layers
517 of Miracloth to remove debris, and protoplast concentration was adjusted to 2-5x10⁵ cells/mL.
518 Protoplasts were then PEG-mediated transformed using 10 µg of indicated effector and reporter

519 plasmids and 2 µg of reference plasmid. After 17 h of incubation at RT, protoplasts were lysed.
520 Firefly (F-LUC) and Renilla Luciferase (R-LUC) activities were measured using Dual
521 Luciferase Reporter Assay System (Promega) and a TECAN Spark 10M 96-well plate reader.
522 F-LUC/R-LUC luminescence ratios were calculated with background-corrected values. Four
523 biological replicates were done for each plasmid combination. All DLRA data were analyzed
524 using R Studio software and are presented as mean ± SD. All statistical methods are indicated
525 within the figure legends. One-way ANOVA was used to analyze experimental data with more
526 than two experimental groups. Welch's ANOVA was performed when the homogeneity of
527 variance assumption was not met. Two-tailed unpaired Student's t-test was used for other data
528 analyses.

529

530 **Electrophoretic Mobility Shift Assay (EMSA).** DNA probes used in EMSA are listed in
531 Supplementary Data 2. Complementary oligos were annealed overnight in annealing buffer (10
532 mM Tris pH 7.5, 150 mM NaCl and 1 mM EDTA). 4 pmol of double-stranded DNA was then
533 fluorescently labeled with 1 unit of Klenow fragment polymerase (NEB) and 8 pmol Cy5-dCTP
534 (Cytiva) in Klenow buffer during 1 h at 37°C. Enzymatic reaction was stopped with a 10-min
535 incubation at 65°C.

536 Proteins used in EMSA were obtained by different methods (bacteria, insect cells or TnT).
537 Recombinant proteins (6xHis-LFY-DBD, UFOΔFbox-3xFLAG) and recombinant complexes
538 (ASK1-UFO, ASK1-UFO-3xFLAG) concentration was adjusted to 500 nM for all reactions.
539 All the 5myc-tagged proteins were obtained in vitro by TnT. 50 µL TnT reactions were done
540 by mixing for 2 h at 25°C 5 µg of pTNT-5myc plasmid containing the gene of interest with
541 TnT SP6 High-Yield Wheat Germ Protein Expression System (Promega). For EMSA with TnT-
542 produced proteins, 5 µL of TnT reaction was used. Recombinant protein buffer or TnT mix was
543 used as control when comparing reactions with multiple proteins.

544 All binding reactions were performed in 20 μ L binding buffer (20 mM Tris pH 7.5, 150 mM
545 NaCl, 1% glycerol, 0.25 mM EDTA, 2 mM MgCl₂, 0,01% Tween-20 and 3 mM TCEP) with
546 10 nM labelled probe. Reactions were supplemented with 140 ng/ μ L fish sperm DNA (Sigma-
547 Aldrich) for EMSAs performed with in vitro-produced LFY, and 200 ng/ μ L for EMSAs
548 performed with recombinant 6xHis-LFY-DBD. Binding reactions were incubated for 20 min
549 on ice and then loaded on a 6 % native polyacrylamide gel. Gels were electrophoresed at 90 V
550 for 75 min at 4°C and revealed with an Amersham ImageQuant 800 imager (Cytiva).
551 Uncropped gels are shown in Source data.

552

553 **Recombinant protein production and purification from bacteria.** 6xHis-LFY-DBD was
554 produced in E.Coli Rosetta2 (DE3) cells (Novagen) and purified as previously described ³⁰.
555 ASK1 was cloned into the pETM-11 expression vector ⁴⁸, and the resulting plasmid was
556 transformed into E.Coli BL21 cells (Novagen). Bacteria were grown in LB medium
557 supplemented with kanamycin and chloramphenicol at 37°C up to an OD_{600nm} of 0.6. Cells were
558 then shifted to 18°C and 0.4 mM isopropyl b-D-1-thiogalactopyranoside (IPTG) was added.
559 After an overnight incubation, cells were sonicated in UFO buffer (25 mM Tris pH8, 150 mM
560 NaCl, 1 mM TCEP) supplemented with one EDTA-free Pierce Protease Inhibitor Tablets
561 (ThermoFisher). Lysed cells were then centrifuged for 30 min at 15000 rpm. Supernatant was
562 mixed with Ni Sepharose High Performance resin (Cytiva) previously equilibrated with UFO
563 buffer (25 mM Tris pH 8, 150 mM NaCl, 1 mM TCEP). Resin was then washed with UFO
564 buffer containing 20 and 40 mM imidazole. Bound proteins were eluted with UFO buffer
565 containing 300 mM imidazole and dialyzed overnight at 4 °C against UFO buffer without
566 imidazole.

567

568 **Recombinant protein production and purification from insect cells.** The different tagged
569 versions of ASK1, LFY and UFO were cloned in acceptor and donor plasmids (pACEBac1,
570 pIDK and pIDS respectively; Geneva Biotech). Final acceptor plasmids containing the
571 combination of desired coding sequences were obtained with Cre recombinase (NEB).
572 DH10EmBacY competent cells containing the baculovirus genomic DNA (bacmid) were
573 transformed with final acceptor plasmids. Blue-white selection was used to identify colonies
574 with a recombinant bacmid with acceptor plasmid inserted. Bacmid was then isolated from
575 bacteria and mixed with X-tremeGENE HP DNA Transfection Reagent (Roche) to transfect
576 Sf21 insect cells. 96 h after transfection, supernatant containing the recombinant baculovirus
577 (V0) was collected and used to infect fresh Sf21 cells. When infected cells reached DPA (Day
578 Post Arrest), V1 virus was collected. For large expression, Sf21 cells were infected with either
579 V1 virus or frozen baculovirus-infected cells. The pellet of a 0.75 L culture was sonicated in 50
580 mL of UFO buffer supplemented with one EDTA-free Pierce Protease Inhibitor Tablets
581 (ThermoFisher). Sonicated cells were centrifuged for 1.5 h at 30 000 rpm, 4 °C. Supernatant
582 was then incubated for 1 h at 4°C with Ni Sepharose High Performance resin (Cytiva)
583 previously equilibrated with UFO buffer. Beads were transferred into a column, and washed
584 with 20 column volumes of UFO buffer, then UFO buffer + 50 mM imidazole. Proteins were
585 eluted with UFO buffer containing 300 mM imidazole. Elution was dialyzed overnight at 4 °C
586 against UFO buffer. TEV protease was added to cleave tags (0.01% w/w). When ASK1 was
587 limiting compared to UFO, recombinant 6xHis-ASK1 from bacteria was added. The following
588 day, elution was repassed on Dextrin Sepharose High Performance (Cytiva) and Ni Sepharose
589 High Performance resins (Cytiva) to remove tags and contaminants. For ASK1-UFO, ASK1-
590 UFO-3xFLAG or UFO Δ Fbox-3xFLAG, proteins were concentrated with a 30 kDa Amicon
591 Ultra Centrifugal filter (Millipore) and further purified by Size Exclusion Chromatography
592 (SEC). For ASK1-UFO-LFY-DBD complex purification, contaminant DNA was removed by

593 passing proteins on Q Sepharose High Performance resin (Cytiva) pre-equilibrated with UFO
594 buffer. Increasing salt concentrations allowed obtaining DNA-free proteins. Indicated annealed
595 HPLC-purified oligos (Supplementary Data 2) were then added and incubated with proteins on
596 ice for 20 min. Proteins were concentrated with a 30 kDa Amicon Ultra Centrifugal filter
597 (Millipore) and further purified by SEC.

598

599 **Size Exclusion Chromatography (SEC) and Size Exclusion Chromatography coupled to**
600 **Multi-Angle Laser Light Scattering (SEC-MALLS).** SEC was performed with a Superdex
601 200 Increase 10/300 GL column (Cytiva) equilibrated with UFO buffer. Unaggregated proteins
602 of interest were frozen in liquid nitrogen and stored at -80°C. SEC-MALLS was performed
603 with a Superdex 200 Increase 10/300 GL column (Cytiva) equilibrated with UFO buffer. For
604 each run, 50 µL containing 1 mg/mL of complex was injected. Separations were performed at
605 RT with a flow rate of 0.5 mL/min. Elutions were monitored by using a Dawn Heleos II for
606 MALLS measurement (Wyatt Technology) and an Optilab T-rEX refractometer for refractive
607 index measurements (Wyatt Technology). Molecular mass calculations were performed using
608 the ASTRA software with a refractive index increment (dn/dc) of 0.185 mL/g.

609

610 **ampDAP-seq.** pTnT-5xmyc-LFY²⁷ was used to produce 5xmyc-LFY in vitro using TnT SP6
611 High-Yield Wheat Germ Protein Expression System (Promega). We used the ampDAP-seq
612 libraries described in Lai et al.²⁷. ampDAP-seq experiments were performed in triplicates (LFY-
613 UFO) or in duplicates (LFY_{K249R} and LFY_{K249R}-UFO).

614 A 50 µL TnT reaction producing 5xmyc-LFY was mixed with an excess of recombinant ASK1-
615 UFO-3xFLAG (2 µg) and 20 µL of Pierce Anti-c-Myc Magnetic Beads (ThermoScientific).
616 DAP buffer (20 mM Tris pH 8, 150 mM NaCl, 1 mM TCEP, 0,005% NP40) was added to reach
617 200 µL. Mix was incubated for 1 h at 4°C on a rotating wheel. Beads were then immobilized

618 and washed 3 times with 100 μ L DAP buffer, moved to a new tube and washed once again.
619 ampDAP-seq input libraries (50 ng) were then added, and protein-DNA mixes were incubated
620 for 1.5 h at 4°C on a rotating wheel. Beads were immobilized and washed 5 times with 100 μ L
621 DAP buffer, moved to a new tube and washed 2 more times. Finally, beads were mixed with
622 30 μ L of elution buffer (10 mM Tris pH 8.5) and heated for 10 min at 90°C.
623 IP-ed DNA fragments contained in the elution were amplified by PCR according to published
624 protocol⁴⁹ with Illumina TruSeq primers. Remaining beads were mixed with 20 μ L of 1X SDS-
625 PAGE Protein Sample Buffer and WB were performed to check the presence of tagged proteins.
626 PCR products were purified using AMPure XP magnetic beads (Beckman Coulter) following
627 manufacturer's instructions. Library molar concentrations were determined by qPCR using
628 NEBNext Library Quant Kit for Illumina (NEB). Libraries were then pooled with equal
629 molarity. Sequencing was done on Illumina HiSeq (Genewiz) with specification of paired-end
630 sequencing of 150 cycles.

631

632 **GUS staining.** The different promoter versions were cloned upstream *GUS* gene in the pRB14
633 backbone vector⁴⁶. Transformants were selected with GFP seed fluorescence. The number of
634 independent lines analyzed for each construct is indicated in each figure. GUS staining was
635 performed on the apex of primary inflorescences of T2 plants. Tissues were placed in ice-cold
636 90% acetone for 20 min at RT, and then rinsed in GUS buffer without X-Gluc (0.2% Triton X-
637 100, 50 mM NaPO₄ pH 7.2, 2 mM potassium ferrocyanide, 2 mM potassium ferricyanide).
638 Tissues were transferred in GUS buffer containing 2 mM X-Gluc substrate (X-Gluc DIRECT)
639 and placed under vacuum for 5 min. Samples were then incubated overnight at 37°C unless
640 specified in the legend. Finally, tissues were washed with different ethanol solutions (35%,
641 50%, and 70%) and pictures were taken with a Keyence VHX-5000 microscope with a VH-

642 Z100R objective. χ^2 tests were used to test for independency between constructs and staining
643 classes.

644

645 ***In planta* overexpression and mutant complementation assay.** Tagged versions of UFO and
646 UFO Δ Fbox were cloned under the control of the 35S promoter in pEGAD⁵⁰. Transformants
647 were selected with Basta treatment. Overexpressing lines with a strong gain-of-function
648 phenotype were crossed to the strong *ufo-1* mutant. Basta-resistant F2 plants were individually
649 genotyped to select *ufo-1* *-/-* homozygous plants. For this, a fragment was amplified by PCR
650 with oligos oGT1085 and oPR578 (Supplementary Data 2) and digested with DpnII enzyme
651 (NEB). Based on digestion profile, *ufo-1* *-/-* plants were kept and analyzed once they reached
652 flowering.

653 Mutated versions of LFY were cloned in pETH29³⁰ or pCA26⁵¹ to express LFY cDNA under
654 the control of its endogenous promoter or the 35S promoter, respectively. For *lfy-12*
655 complementation assay, heterozygous *lfy-12/+* plants were transformed. Transformants were
656 selected with GFP fluorescence and genotyped with a previously described protocol⁴⁶ to select
657 *lfy-12* *-/-* plants. Complementation assay was performed with T2 plants and was based on the
658 analysis of the first 10 flowers from the primary inflorescence. Pictures were taken with a
659 Keyence VHX-5000 microscope with a VH-Z20R objective. χ^2 tests were used to test for
660 independency between constructs and complementation classes.

661 .

662

663

664 **Western Blot.** For Western Blots on plant total protein extracts, indicated tissues were crushed
665 in 2X SDS-PAGE Protein Sample Buffer (100 mM Tris pH 6.8, 20% glycerol, 2% SDS, 0.005%
666 Bromophenol blue, and 0.8% w/v dithiothreitol) at a 1:2 w:v ratio and boiled for 5 min. Samples

667 were then loaded on a 12% acrylamide SDS-PAGE gel. For all WB, transfer was performed
668 with iBlot2 Dry Blotting System (Invitrogen) using default parameters. Membranes were
669 blocked for 1 h at RT with 5% milk TBST and then incubated overnight at 4 °C with 5% milk
670 TBST solution containing HRP-conjugated antibody (1:1000 for anti-FLAG (Sigma-Aldrich;
671 Cat# A8592) and 1:5000 for anti-myc (Invitrogen; Cat# R951-25)). Revelation was performed
672 with Clarity Western ECL substrate (Bio-Rad). Pictures were taken with a ChemiDoc MP
673 Imaging System (BioRad). Uncropped gels are shown in Source Data.

674

675 **Cryo-EM sample preparation, data collection and data processing.** An aliquot of the SEC-
676 purified ASK1-UFO-LFY-LUBS1 complex was thawed on ice (see Supplementary Data 2 for
677 LUBS1 DNA sequence). Subsequently, 3.5 μ l of the complex at 1 mg/mL were deposited onto
678 glow-discharged (25 mA, 30 s) C-flat Au grid R 1.2/1.3 300 mesh (Electron Microscopy
679 Sciences), blotted for 5.5 s with force 0, at 20°C and 100% humidity using a Mark IV Vitrobot
680 (FEI, Thermo Fisher Scientific) and plunge-frozen in liquid ethane for specimen vitrification.
681 A dataset of about 1'000 movies of 40 frames was acquired on a 200 kV Glacios (Thermo
682 Fisher Scientific) electron microscope (Supplementary Data 3) at a nominal magnification of
683 36'000 with a physical pixel size of 1.145 Å.

684 The raw movies, acquired with SerialEM on a Gatan K2 Summit camera (Supplementary Data
685 3), were imported to Cryosparc live⁵² for motion correction and CTF estimation. The dose-
686 weighted micrographs were used for particle picking with crYOLO 1.7.6 and the general model
687 for low-pass filtered images⁵³. Particle coordinates were imported to Cryosparc, where all
688 subsequent steps were performed. After manual inspection, a subset of 761 micrographs was
689 selected based on CTF fit resolution, total and per frame motion, average defocus and relative
690 ice thickness. A raw particle stack of 282'567 images was extracted at 256x256 pixels² box size,
691 binned twice and subjected into 2D classification to remove false positive picks. 207'392

692 particles from the selected class averages were re-extracted, re-centered at full size and
693 submitted for a second round of 2D classification. All class averages showing clear protein
694 features were selected and the resulting 147'849 particles were used for ab initio reconstruction
695 with 3 classes and subsequent heterogeneous refinement of the resulting volumes. Of those 3
696 classes, 2 looked like a protein-DNA complex with the most apparent difference being the
697 presence or not of an extra electron density at one edge of the DNA helix. The last class had no
698 recognizable features and was used as a decoy to remove "junk" particles. Each subset and
699 volume of the 2 first classes was refined separately with Non-Uniform refinement⁵⁴ resulting
700 into 2 distinct reconstructions of about 4.2 Å resolution, where the DNA model, the crystal
701 structure of LFY-DBD and the AlphaFold2 models of UFO and ASK1 could be unambiguously
702 fitted into the electron density. The second of these classes could fit a LFY-DBD dimer, while
703 in the first class there was density only for the LFY-DBD molecule that directly interacts with
704 UFO (Extended Data Fig. 9d). The unsharpened maps of each reconstruction were used for
705 post-processing with DeepEMhancer⁵⁵. Figures were prepared with Chimera⁵⁶ or ChimeraX⁵⁷.

706

707 **Cryo-EM model building.** Ideal B-form DNA was generated in Coot⁵⁸ and then manually built
708 into the electron density. The resulting model was further refined using
709 phenix.real_space_refine⁵⁹. A single monomer of LFY-DBD was manually placed in the
710 electron density, followed by fitting in ChimeraX⁵⁷. The biological LFY-DBD dimer was then
711 downloaded from the RCSB PDB (2VY1)³⁰ and used as a guide to place the second LFY
712 monomer, followed by fitting to density in ChimeraX. Alphafold models⁶⁰ of ASK1 (uniprot
713 ID: Q39255) and UFO (uniprot ID: Q39090) were both downloaded from the EBI, preprocessed
714 to remove low confidence regions in phenix.process_predicted_model⁶¹, then placed manually
715 and then fit to density in ChimeraX.

716

717 **Bioinformatic analyses.**

718 *Read mapping and peak calling.* Reads processing and peak calling of LFY, LFY-UFO,
719 LFY_{K249R} and LFY_{K249R}-UFO ampDAP-seq data were performed as previously published⁶².
720 Briefly, the quality of sequencing data was analyzed with fastQC v0.11.7 and adapters were
721 removed with NGmerge v0.2_dev⁶³. Bowtie2 v2.3.4.1 was used for mapping to the TAIR10 A.
722 *thaliana* reference genome⁶⁴. Reads mapped to a single location and with maximum two
723 mismatches were retained Duplicates were removed with the samtools dedup program v1.8.
724 Bound regions (i.e. peaks) were identified with MACS2 v2.2.7.1, using input DNA from Lai et
725 al. as control²⁷. Consensus peaks were selected with MSPC v4.0.0⁶⁵ by retaining peaks called
726 in all replicates, and resizing them by ± 200 bp around the peak maximum for further analysis.

727

728 *Analyses of ampDAP-seq experiments.* To compare binding in different experiments, peaks
729 were merged according to a previously published procedure⁶². Bound peaks were considered as
730 common if they overlapped by at least 80%, while the remaining non-overlapping portion of
731 either peak was $< 50\%$. Peaks that did not overlap by at least 50% were considered as new
732 peaks. The same procedure was used to assess experimental reproducibility (comparisons
733 between replicates of the same experiment), where peaks were normalized by the number of
734 reads mapped in library (RPKM).

735 As the fraction of reads mapped in peaks is much lower for LFY than LFY-UFO ampDAP-seq
736 ($\sim 25\%$ vs $\sim 40\%$, respectively), normalizing reads count by all reads mapped along the genome
737 would introduce a bias and estimate the LFY relative coverage (RPKM) towards lower values
738 compared to LFY-UFO. In addition to this consideration, experimental proof from EMSAs
739 suggests that UFO does not strongly affect binding intensity of the complex at canonical
740 LFYBS (which represent most peaks). Hence, reads count at each peak was normalized by the
741 total number of reads mapped within all LFY and LFY-UFO merged peaks. Then, the mean

742 normalized coverage from each experiment, divided by the peak size, was computed for each
743 peak. The same strategy was applied when comparing LFY_{K249R} and LFY_{K249R}-UFO (Fig. 4b),
744 LFY_{K249R} and LFY (Extended Data Fig. 8h) and LFY, LFY-UFO, LFY_{K249R} and LFY_{K249R}-
745 UFO (Fig. 4c). The Coverage Fold Change (CFC) was computed on merged peaks as the ratio
746 between mean normalized peak coverage in LFY-UFO and LFY (Fig. 2d) or mean normalized
747 coverage in LFY_{K249R}-UFO and LFY_{K249R} (Fig. 4b).

748

749 *Motif search in bound regions.* Merged peaks of LFY and LFY-UFO datasets were sorted based
750 on decreasing CFC value. The top 600 peaks (i.e. highest CFC values) were used for a motif
751 search using MEME-ChIP v4.12.0 using options -nmeme 600 -meme-maxsize 600*1000 -
752 meme-nmotifs 1 -dreme-m 0 -noecho and the JASPAR 2018 core plants non-redundant
753 database⁶⁶. For dLUBS, we used options -meme-minw 20 -meme-maxw 30, while for mLUBS
754 we used -meme-minw 16 -meme-maxw 19. To retrieve the LFY motif in Fig. 2e the 600 LFY
755 ampDAP-seq peaks with strongest coverage were fed to MEME-ChIP with options -nmeme
756 600 -meme-nmotifs 1 --meme-minw 19 -meme-maxw 19 -pal.

757

758 *Receiver Operating Characteristics (ROC) analysis.* From the dataset of merged peak set
759 (peaks found in LFY or in LFY-UFO experiments or in both), peaks were sorted based on
760 decreased CFC value, the top 20% peaks were selected, and among these, the first 600 used for
761 motif determination were excluded to avoid overfitting, for a total of 3243 final peaks. A
762 negative set of the same size was created using a previously published method, which allows
763 searching for sequences from the *A. thaliana* genome (TAIR10 reference) with the same GC
764 content and genomic origin as the positive set⁶⁷. Both sets were scanned with dLUBS and
765 mLUBS PWMs as well as with the LFY PWM with dependencies as published previously⁶⁸

766 using an in-house script available on our GitHub page. The ROC plot was then created with the
767 R 'plotROC' package v2.2.1.

768

769 *LFY in dLUBS within LFY-UFO-specific regions vs LFY in LFY-specific regions.* To assess
770 whether the scores of LFYBS within dLUBS were comparable to the scores of canonical
771 LFYBS, we used the peaks from the comparison of LFY vs LFY-UFO ampDAP-seq and
772 resized them (+/-50 bp around the peak maximum). We used the dLUBS matrix to scan the
773 resized sequences and retained the best site per sequence. We then retrieved sequences
774 corresponding to the dLUBS site and computed the score of the LFYBS present in dLUBS
775 using the LFY PWM⁶⁸. The values obtained in the 20% most LFY-UFO-specific sequences
776 (20% highest CFC) is shown in the boxplot. The 20% lowest CFC peaks were scanned with the
777 LFY PWM to generate the box-plot in Extended Data Fig. 4f.

778

779 *Microarray data analysis.* Microarray data were retrieved from AtGenExpress⁶⁹ for
780 inflorescence tissue in the *ufo* (ATGE_52A-C) vs Col-0 background (ATGE_29A-C). The
781 'gcrma' R package was used to adjust probe intensities and convert them to expression
782 measures, and then the 'limma' package was used to fit the model and smooth standard errors.
783 A Benjamini-Hochberg correction was applied to p-values and fold change (FC) was computed
784 as the ratio between expression in WT versus the *ufo* mutant. Only genes with $|\log_2(\text{FC})| > 0.5$
785 and adjusted p-value < 0.05 were considered as significantly differentially expressed.

786

787 *ChIP-seq datasets and analysis of ChIP-seq vs ampDAP-seq.* We collected the raw data of all
788 available LFY ChIP-seq datasets: GSE141704⁷⁰, GSE96806²⁵, GSE64245²⁶, GSE24568⁶⁸.
789 Mapping and peakcalling analysis were performed with the same procedure as ampDAP-seq,
790 except that peaks were resized to 600 bp around the peak maximum, and the -q option of

791 MACS2 was set to 0.1. Coverage of the resulting peaks was calculated as the average of
792 normalized read coverage for each replicate. Peaks from the four datasets were merged through
793 a four-way comparison following the same procedure used for ampDAP-seq. Bedtools intersect
794 (v2.30.0) was used with options -wa -f 0.8 -F 0.8 -e to find the peaks common to the merged
795 ChIP-seq peaks and the 20% most LFY-UFO-specific genomic regions (highest CFC value
796 from ampDAP-seq). Peaks were assigned to genes by extending gene regions 3 kb upstream of
797 the TSS and 1 kb downstream of the TTS and using bedtools intersect (options -f 0.8 -F 0.8 –
798 e) to identify genes in the vicinity of peaks. The bound genes obtained were crossed with the
799 list of differentially expressed genes in *ufo* inflorescences.

800

801 *Identification of the URM from published LFY ChIP-seq data.* To test whether the URM could
802 be identified *de novo* (Extended Data Fig. 4g), we collected the 298 regions bound by LFY
803 ChIP-seq data of inflorescence tissue²⁵ for which the binding intensity was twice greater in vivo
804 relative to in vitro (LFY ampDAP-seq). We resized these regions +/- 55 bp around the ChIP-
805 seq peak maximum. The corresponding sequences were searched with the LFY PWM⁶⁸ to
806 identify all LFYBS with a PWM score > -23. Assuming that a recruiting motif should be at a
807 fixed distance from the LFYBS, we created 140 batches, corresponding to sequences with size
808 ranging from 4 to 10 bp, distant from 1 to 20 bp at both sides of the canonical LFYBS. Each of
809 the 140 batches of sequences was used as input with MEME-ChIP for motif discovery with the
810 motif size constrained to the length of the sequences in a given batch.

811

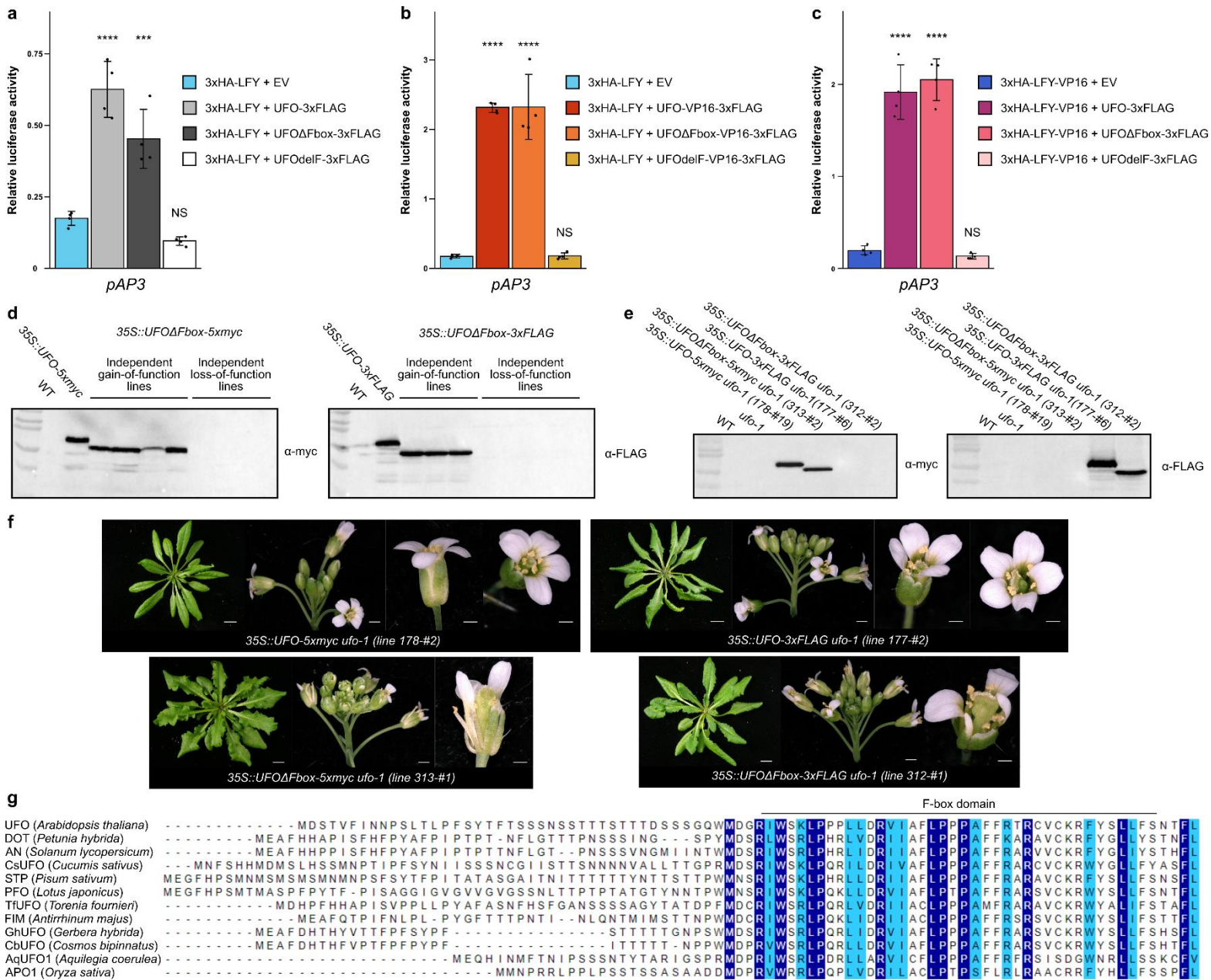
812 **Data and code availability**

813

814 ampDAP-seq data have been deposited at GEO and are publicly available as of the date of
815 publication (GSE204793; reviewer link: mlufkwogxjurvcj). All original code has been

816 deposited at github (https://github.com/Bioinfo-LPCV-RDF/LFYUFO_project) and is publicly
817 available as of the date of publication. The cryo-EM structure determined in this study is
818 deposited in the EM data bank under the reference number EMD-15145. The .pdb file of the
819 model is available in Supplementary information. Any additional information required to
820 reanalyze the data reported in this paper is available from the lead contact upon request.
821

822 **Extended Data Figures**



823

824 **Extended Data Fig. 1. UFO has SCF-dependent and independent functions. a-c, *pAP3***

825 activation measured by DLRA in Arabidopsis protoplasts. EV = Empty Vector (pRT104-

826 3xHA). UFOΔFbox corresponds to a deletion of the whole N-terminal part comprising the F-

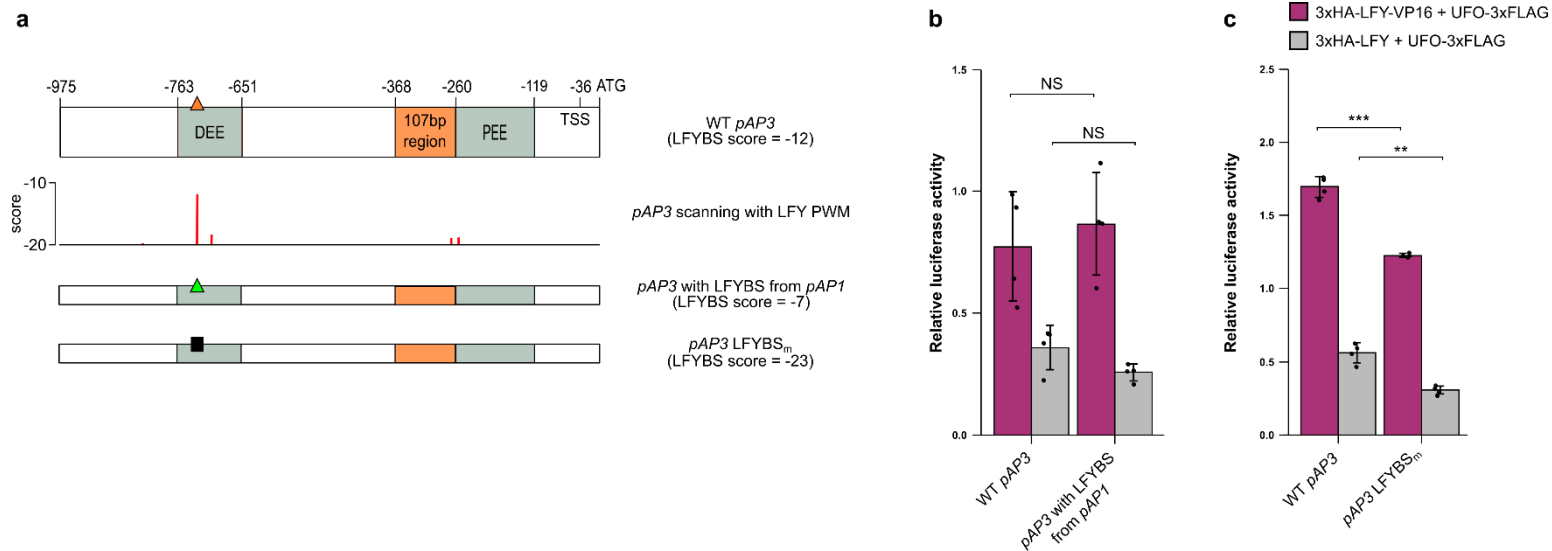
827 box domain (aa. 1-90), while UFOdelF corresponds to a previously-described internal deletion

828 in the F-box domain (aa. 50-62)²⁰. Data represent averages of independent biological replicates

829 and are presented as mean ± SD, each dot representing one biological replicate (n = 4). One-

830 way ANOVA with Tukey's multiple comparisons test. Stars above bars represent a significant
831 statistical difference compared to 3xHA-LFY + EV or 3xHA-LFY-VP16 + EV negative
832 controls (NS: $p > 0.05$, *: $p < 0.05$, **: $p < 0.01$, ***: $p < 0.001$ and ****: $p < 0.0001$). **d**,
833 Western Blot on protein extracts from independent T1 plants from different phenotypic classes
834 described in Fig. 1g (one independent line per lane). *35S::UFO-5xmyc* (line 178-#19) and
835 *35S::UFO-3xFLAG* (line 177-#6) plants were used as positive controls. Total proteins were
836 extracted from rosette leaves. Note the difference of molecular weight between UFO and
837 $UFO\Delta Fbox$. Loss-of-function defects are likely due to silencing of both transgene-encoded
838 $UFO\Delta Fbox$ and endogenous UFO. **e**, Western Blot on protein extracts from F2 plants described
839 in Fig. 1h. Total proteins were extracted from rosette leaves. **f**, *ufo-1* complementation assay
840 with other *35S::UFO* and *35S::UFO\Delta Fbox* lines. Rosette leaves (right, scale bar, 1 cm),
841 inflorescence (middle, scale bar 1 mm) and flower (right, scale bar, 0.5 mm) phenotypes are
842 shown. Primary inflorescences were removed to observe rosette phenotype. For each construct,
843 at least 5 plants were analyzed per line. As in Risseuw et al, our *35S::UFO* lines displayed
844 relatively milder phenotypes than the *35S::UFO* phenotypes reported by Lee et al.^{6,20}. Note that
845 the *35S::UFO-5xmyc* 178-#2 line did not display the serrated leaves phenotype. **g**, Sequence
846 alignment of UFO N-terminal region. The F-box domain is represented⁷¹. In selected species,
847 presented proteins were identified as UFO homologs and their role was confirmed
848 genetically^{7,11,12,16,72-79}.

849



850

851 **Extended Data Fig. 2. *pAP3* DEE LFYBS is not required for LFY-UFO-dependent *pAP3***

852 **activation. a**, Schematic representation of *pAP3*. Top row represents WT *pAP3* with regulatory

853 regions and *cis*-elements. Orange triangle represents LFYBS. The second row represents the

854 scores for the best LFYBS obtained by scanning WT *pAP3* sequence with LFY PWM⁶⁸ (the

855 best binding sites correspond to the less negative score values). Other rows represent the

856 different *pAP3* versions used in (b) and (c). LFYBS mutation corresponds to the previously

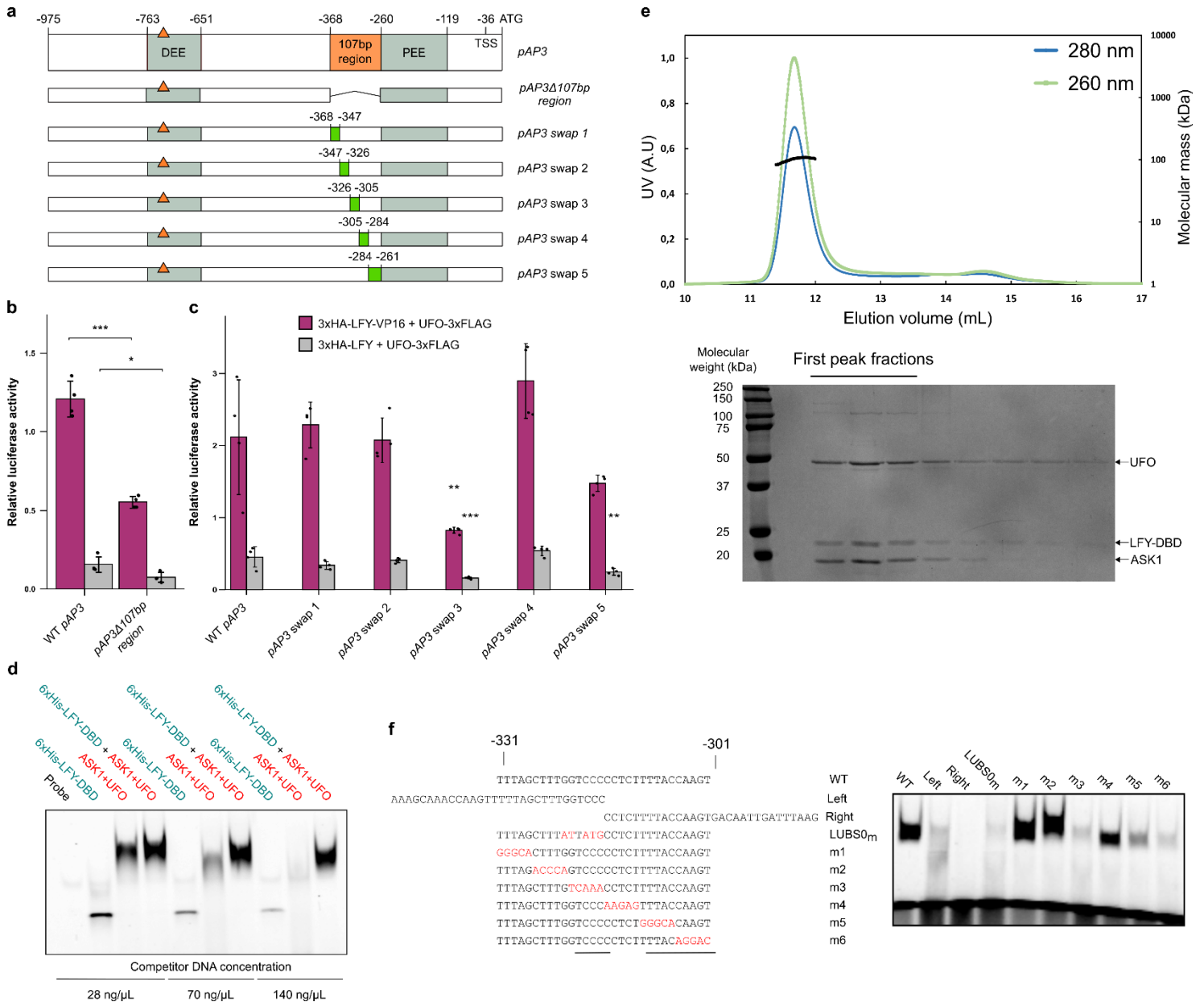
857 described *site1m-site2m* mutation²⁴. b,c, *pAP3* activation with promoter versions described in

858 (a) and indicated effectors. For bar charts, data represent averages of independent biological

859 replicates and are presented as mean \pm SD, each dot representing one biological replicate (n =

860 4). Unpaired t-tests (b,c). (NS: $p > 0.05$, *: $p < 0.05$, **: $p < 0.01$, ***: $p < 0.001$).

861



862

863 **Extended Data Fig. 3. Analysis of *pAP3* activation by LFY-UFO. a**, Description of *pAP3*.

864 Top line represents WT *pAP3* with regulatory regions and *cis*-elements. Coordinates are relative

865 to *AP3* start codon. TSS: Transcription Start Site. Orange triangle represents LFYBS. Other

866 rows show the promoter versions used in (b) and (c). Green rectangles in swapped versions

867 correspond to the same random sequence. b,c, *pAP3* LFY-UFO response element mapping

868 with *pAP3* versions described in (a) by DLRA in *Arabidopsis* protoplasts. Data represent

869 averages of independent biological replicates and are presented as mean \pm SD, each dot

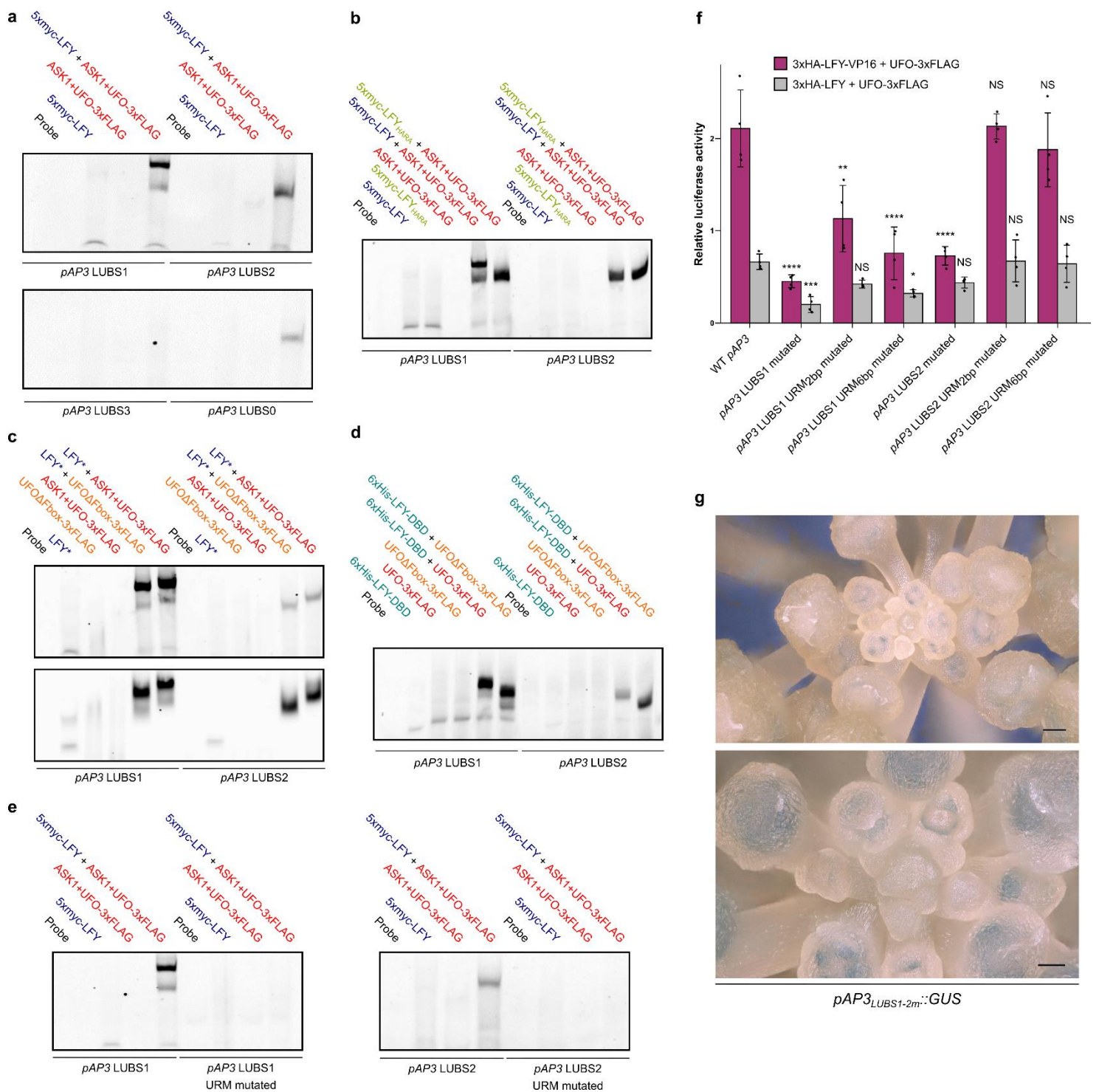
870 representing one biological replicate ($n = 4$). One-way ANOVA with Tukey's multiple
871 comparisons test (c). One-way ANOVA was performed with data from the same effector, and
872 stars represent a statistical difference compared to WT *pAP3*. Unpaired t-test (b). (NS: $p >$
873 0.05 ,*: $p < 0.05$, **: $p < 0.01$; ***: $p < 0.001$). **d**, EMSA with ASK1-UFO, LFY-DBD and
874 LUBS0 DNA probe. Different competitor DNA concentrations were tested as indicated. **e**,
875 Molecular mass determination for ASK1-UFO-LFY-DBD in complex with LUBS0 DNA by
876 SEC-MALLS (top). Elution profiles correspond to absorbance at 280 nm and 260 nm (left
877 ordinate axis, A.U: Arbitrary Unit). The black line shows the molecular mass distribution (right
878 ordinate axis). A mass of 102 ± 3.3 kDa was found for this ASK1-UFO-LFY-DBD-LUBS0
879 complex, consistent with one copy of each protein per DNA molecule (theoretical mass of 108
880 kDa). Coomassie-stained SDS-PAGE gel of the different SEC-MALLS fractions (bottom).
881 Each lane corresponds to a 0.5 mL fraction. Molecular weights of the protein standards are
882 indicated (BioRad Precision Plus). Faint bands above UFO likely correspond to contaminants.
883 **f**, EMSA with ASK1-UFO, LFY-DBD and indicated DNA probes. Sequences with coordinates
884 relative to *AP3* start codon (left). Red letters indicate mutated bases. Bars under sequences
885 represent the regions required for ASK1-UFO-LFY-DBD binding. EMSA with described DNA
886 probes (right). Each DNA probe was mixed with the same ASK1-UFO-LFY-DBD protein mix.
887 Note that the LUBS0 mutation also reduced *pAP3* activation in protoplasts (Fig. 2b).
888

890 **Extended Data Fig. 4. Genome-wide analysis of LFY-UFO binding.** **a**, Western Blot after
891 DNA elution during ampDAP-seq experiment. After DNA elution, 20 μ L of 1X SDS-PAGE
892 Protein Sample Buffer was added to the remaining beads to run WB. Each lane represents one
893 replicate. **b**, Assessment of experimental reproducibility of ampDAP-seq experiment through
894 the comparison of replicates datasets 2 by 2. **c**, Effect of the LFY KARA mutation (K303A-
895 R233A)⁵¹ on *pAP3* activation in Arabidopsis protoplasts. Data represent averages of
896 independent biological replicates and are presented as mean \pm SD, each dot representing one
897 biological replicate (n = 4). Unpaired t-tests (**: p < 0.01; ****: p < 0.0001). **d**, The LFY
898 KARA mutation (K303A-R233A) does not disrupt LFY-UFO interaction in Yeast-Two-Hybrid
899 (Y2H). EV = Empty Vector. LFY-40 is a LFY version lacking the first 40 aa and better tolerated
900 by yeast cells. Values correspond to the different dilutions (OD = 7, 0.7 and 0.07). Top picture
901 corresponds to the non-selective plate lacking Leucine and Tryptophan (SD -L-W), and bottom
902 picture to the selective plate lacking Leucine, Tryptophan, Histidine and Adenine (SD -L-W-
903 A-H). Pictures were taken at day + 4. **e**, Receiver operating characteristics (ROC) curves for
904 mLUBS, dLUBS and LFY using the top 20% high-CFC LFY-UFO-specific peaks. Area under
905 the curve (AUC) values are shown. TPR: True Positive Rate, FPR: False Positive Rate. **f**, Score
906 distribution of LFY PWM with dependencies⁶⁸ within dLUBS (best site on 20% most LFY-
907 UFO-specific genomic regions, high CFC, n = 3843 genomic regions) and in canonical LFYBS
908 (best site on 20% most LFY-specific genomic regions, low CFC, n = 3843 genomic regions).
909 Best sites were selected within \pm 25 bp around the peak maximum. Wilcoxon rank sum test
910 (****: p < 0.0001). Median (solid line), interquartile range (box edges), \pm 1.5 \times interquartile
911 range (whiskers) and outliers (black dot) are shown. **g**, *De novo* identification of URM from
912 LFY ChIP-seq data²⁵. Motifs identified at a fixed distance from LFY canonical binding sites in
913 298 regions harboring high LFY ChIP-seq to LFY ampDAP-seq coverage ratio. The text above
914 each motif gives the motif's start position relative to the canonical LFYBS, its length and the

915 number of sites used to build the motif. **h**, EMSA with mLUBS and dLUBS highest score
916 sequences. 6xHis-LFY-DBD is recombinant. UFO* refers to either recombinant ASK1-UFO-
917 3xFLAG complex (top gel) or *in vitro* produced UFO-3xFLAG (bottom gel). Drawings
918 represent the different types of complexes involving LFY-DBD (pale blue) and ASK1-UFO
919 (red) on DNA. LFY-DBD binds as a monomer as previously reported³⁰. The fact that *in vitro*
920 produced UFO-3xFLAG shifts DNA in the presence of LFY indicates that ASK1 is not required
921 for the UFO-LFY-DNA complex formation *in vitro*. **i**, EMSA with DNA probes corresponding
922 to *pAP1* and *pAP3* DEE LFYBS and indicated proteins. Note that probes used here have the
923 same length as those used to study LUBS.

924

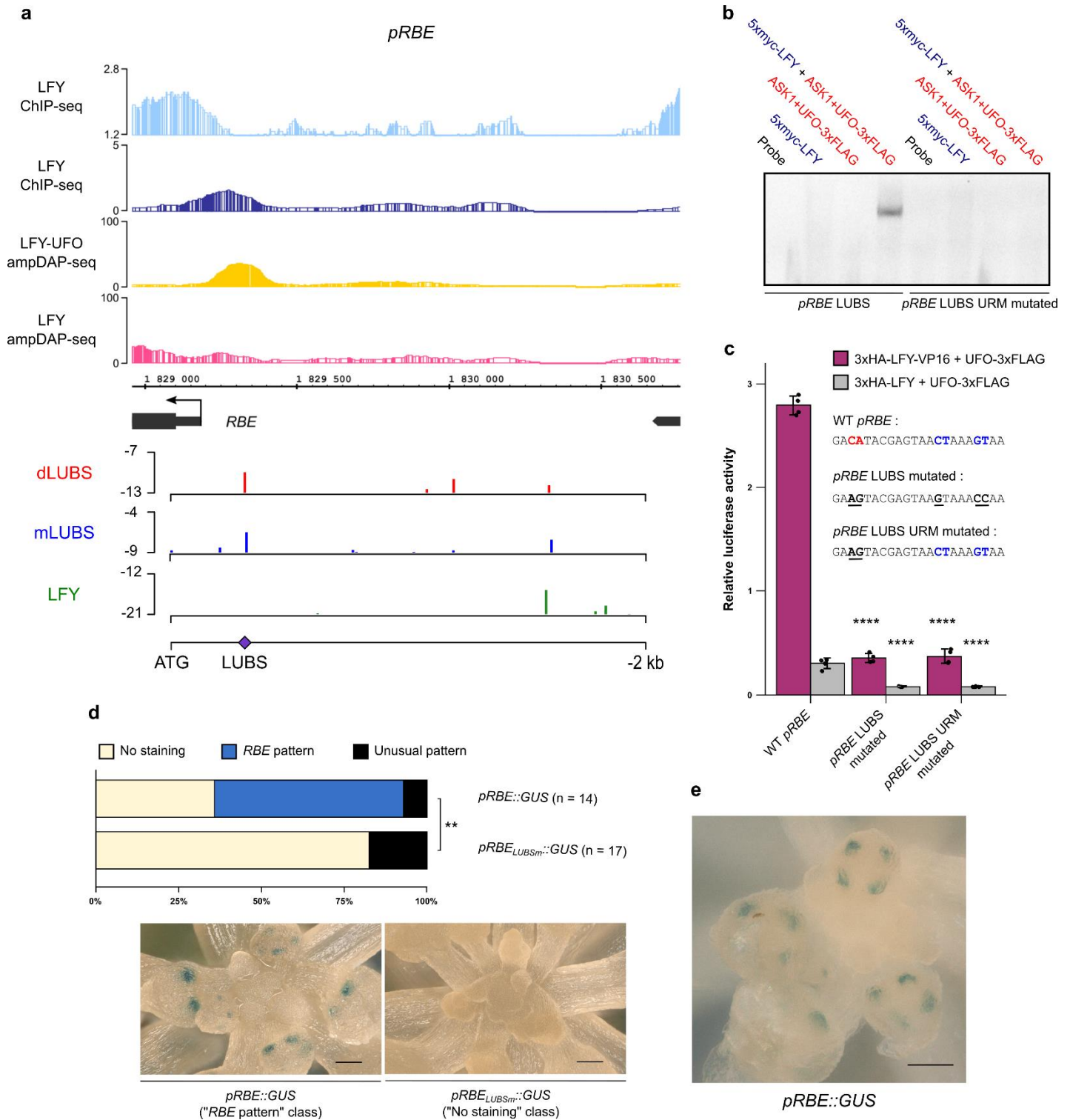
925



926

927 **Extended Data Fig. 5. *pAP3* LUBS are required for LFY-UFO-dependent activation. a,**
 928 **EMSA with indicated probes and proteins. LUBS3 is the third highest-score *pAP3* LUBS.**
 929 **Because LUBS0 is bound with a lower affinity by LFY-UFO compared to LUBS1 and LUBS2,**
 930 **we then focused on LUBS1 and LUBS2. b, EMSA with *pAP3* LUBS1 and LUBS2 DNA probes**

931 and indicated proteins. LFY_{H383A-R386A} (LFY_{HARA}) is a LFY mutated version affected in its
932 ability to dimerize^{30,51}. Note the absence of the complex with a slower mobility on LUBS1 with
933 LFY_{HARA}. **c**, EMSA with *pAP3* LUBS1 and LUBS2 DNA probes and indicated proteins. LFY*
934 refers to either *in vitro*-produced 5xmyc-LFY (top) or recombinant 6xHis-LFY-DBD (bottom).
935 Note the difference of complex size between UFO and UFO Δ Fbox. **d**, Same as in (c) except
936 that UFO-3xFLAG and UFO Δ Fbox-3xFLAG were produced *in vitro*. Note that *in vitro*
937 produced UFO-3xFLAG and UFO Δ Fbox-3xFLAG behave similarly as recombinant UFO
938 versions. **e**, EMSA with indicated proteins and DNA probes corresponding to *pAP3* LUBS1
939 (left) and LUBS2 (right), WT or with URM mutated. **f**, Promoter activation measured by DLRA
940 in Arabidopsis protoplasts with indicated effectors. Different promoter versions were tested as
941 indicated under x-axis. Either 2 bp (high-informative CA) or 6 bp (whole URM) of *pAP3*
942 LUBS1 and LUBS2 URM were mutated. Data represent averages of independent biological
943 replicates and are presented as mean \pm SD, each dot representing one biological replicate (n =
944 4). One-way ANOVA with Tukey's multiple comparisons tests. One-way ANOVA were
945 performed with data from the same effector and stars represent a statistical difference compared
946 to WT *pAP3* promoter. (NS: p > 0.05, *: p < 0.05, **: p < 0.01, ***: p < 0.001 and ****: p <
947 0.0001). **g**, *In vivo* analysis of *pAP3*_{LUBS1-2m}::*GUS* fusions. Same as in Fig. 3d, except that
948 staining incubation time was increased to 17 h (4h incubation in Fig. 3d). Representative
949 pictures are shown (top scale bar, 100 μ m, bottom scale bar, 50 μ m). The faint *AP3* pattern
950 suggests that other LUBS (such as LUBS0) may take over but less efficiently. Note that with
951 this staining incubation time, all plants expressing *pAP3*::*GUS* showed a highly saturated
952 staining.
953



954

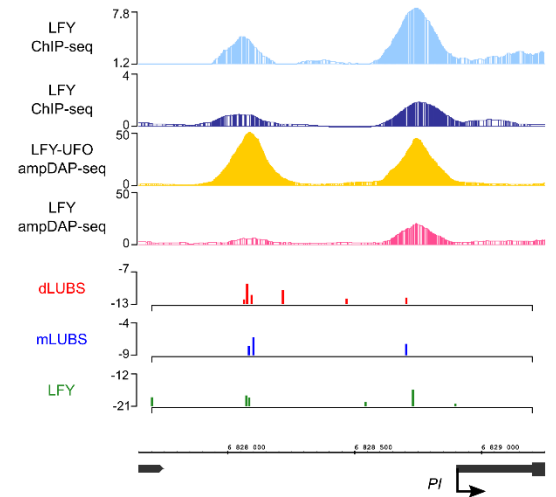
955 **Extended Data Fig. 6. *pRBE* LUBS is required for LFY-UFO-dependent activation.** **a**, IGB
 956 view of *pRBE* showing LFY ChIP-seq in inflorescences (light blue)²⁵ or seedlings (dark blue)²⁶,
 957 LFY-UFO ampDAP-seq (yellow), LFY ampDAP-seq (pink)²⁷, numbers indicate read number
 958 range (top). Identification of LUBS in *pRBE* (bottom). Predicted binding sites using dLUBS

959 and mLUBS models from Fig. 2e and LFY PWM with dependencies⁶⁸, y-axis represents score
960 values (bottom). The best binding sites correspond to the less negative score values. Studied
961 LUBS is indicated with a purple square. **b**, EMSA with probes corresponding to *pRBE* LUBS,
962 WT or with URM mutated. **c**, *pRBE* activation in Arabidopsis protoplasts. Effect of mutations
963 (underlined) in URM (red) and in LFYBS (blue) bases of *pRBE* LUBS were assayed. Data
964 represent averages of independent biological replicates and are presented as mean \pm SD, each
965 dot representing one biological replicate (n = 4). One-way ANOVA with Tukey's multiple
966 comparisons test. One-way ANOVA were performed with data from the same effector, and
967 stars represent a statistical difference compared to WT promoters (****: p < 0.0001). **d**, *In vivo*
968 analysis of *pRBE::GUS* fusions. The percentage of transgenic lines with *RBE* pattern, unusual
969 pattern or absence of staining was scored (top; χ^2 test, **: p < 0.01). n = number of independent
970 lines. Unusual pattern refers to staining in unexpected tissues, each pattern seen in a single line.
971 Representative pictures of plants with no staining (bottom left) and a *RBE* pattern (bottom right)
972 are shown (scale bar, 50 μ m). **e**, *In vivo* analysis of *pRBE::GUS* fusions. Same as in (**d**), with
973 another view showing staining in the four petal primordia (scale bar, 50 μ m).
974

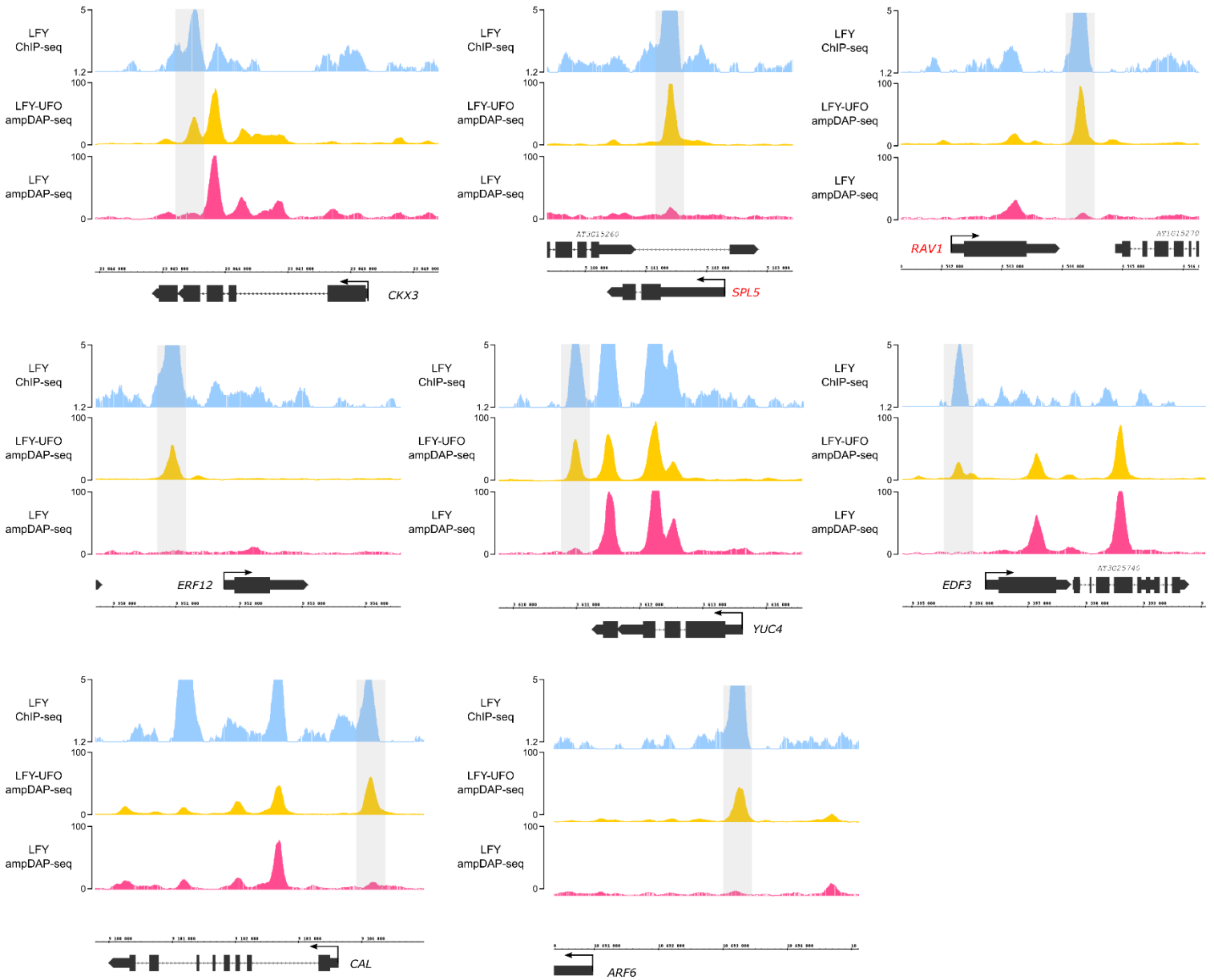
a

Gene	Name	Description	Up/Down regulated	LFY ChIP-Seq set
AT1G13260	RAV1	related to ABI3/VP1 1	down	A
AT1G24530	NA	Transducin/WD40 repeat-like superfamily protein	down	B
AT1G34110	NA	Leucine-rich receptor-like protein kinase family protein	up	C; B
AT1G54010	NA	GDSL-like Lipase/Acylhydrolase superfamily protein	down	A
AT1G73805	NA	Calmodulin binding protein-like	down	C; B; A
AT1G74440	NA	Protein of unknown function (DUF962)	down	A
AT1G75450	ATCKX5	cytokinin oxidase 5	up	C; B; D
AT1G76110	NA	HMG (high mobility group) box protein with ARID/BRIGHT DNA-binding domain	up	A
AT1G80840	ATWRKY40	WRKY DNA-binding protein 40	up	C; B; A
AT3G15270	SPL5	squamosa promoter binding protein-like 5	up	A
AT3G20810	NA	2-oxoglutarate (2OG) and Fe(II)-dependent oxygenase superfamily protein	up	A
AT3G28180	ATCSC04	Cellulose-synthase-like C4	down	B
AT3G54340	AP3	K-box region and MADS-box transcription factor family protein	up	B
AT3G55560	AGF2	AT-hook protein of GA feedback 2	up	C; B; A
AT4G00730	ANL2	Homeobox-leucine zipper family protein / lipid-binding START domain-containing protein	up	A
AT4G02380	AILEA5	senescence-associated gene 21	down	B
AT4G34160	CYCD3	CYCLIN D3	up	A
AT4G35900	FD	Basic-leucine zipper (bZIP) transcription factor family protein	down	C; B; A
AT5G02540	NA	NAD(P)-binding Rossmann-fold superfamily protein	up	B; D
AT5G20240	PI	K-box region and MADS-box transcription factor family protein	up	A

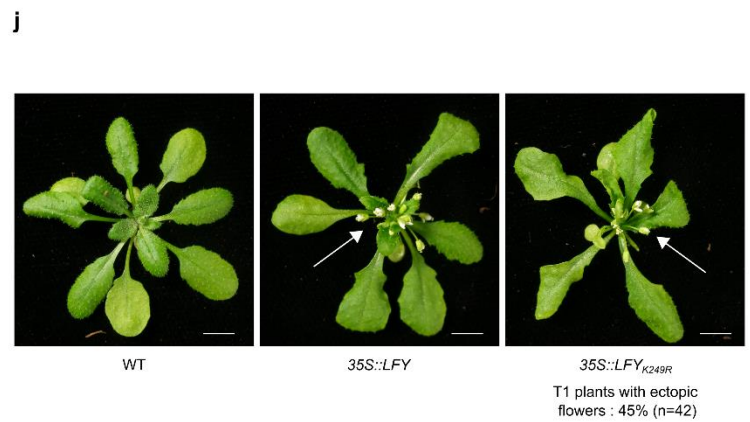
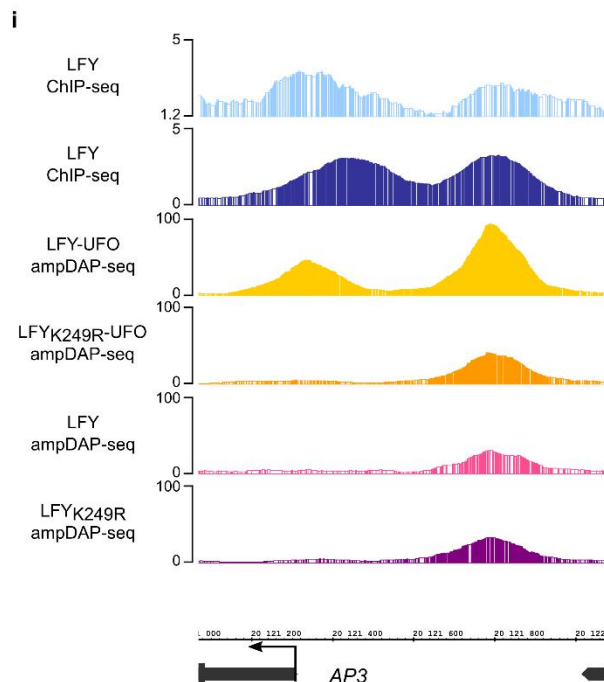
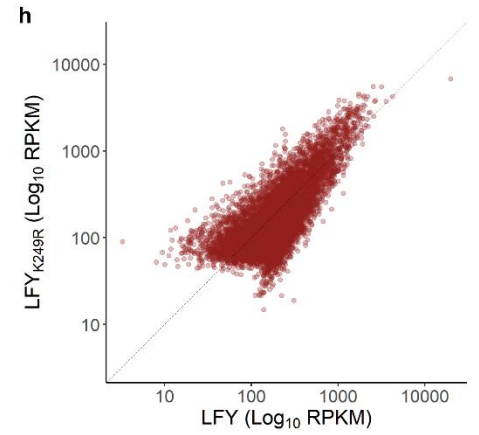
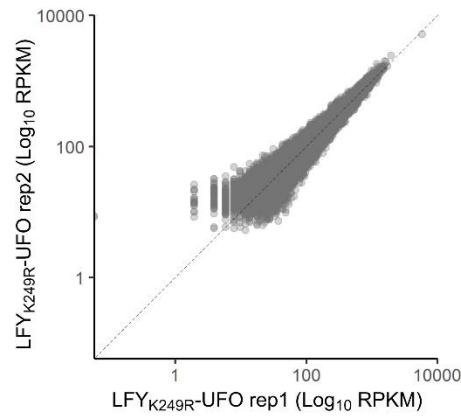
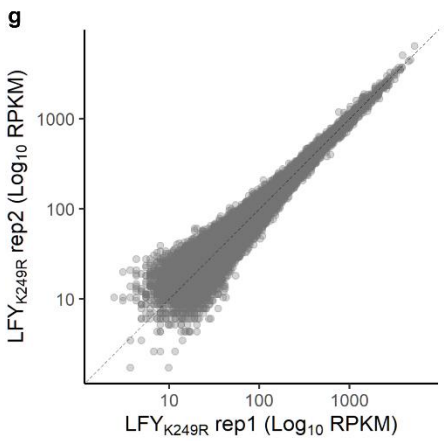
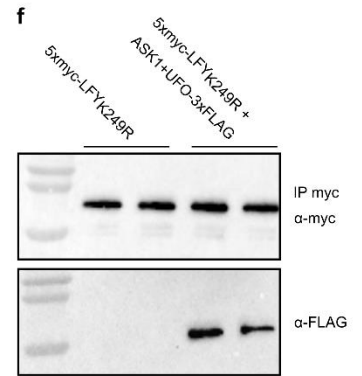
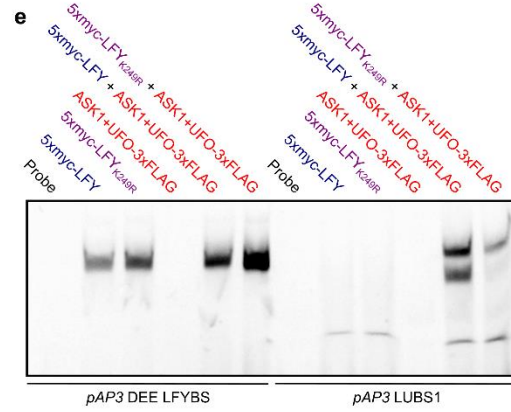
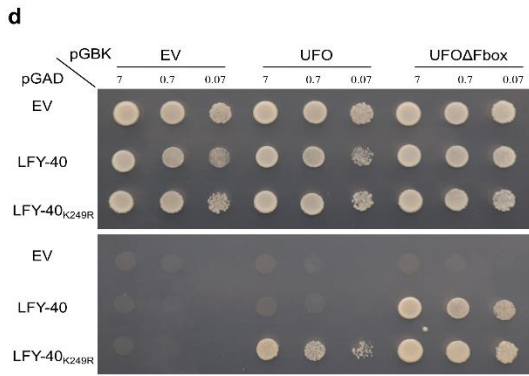
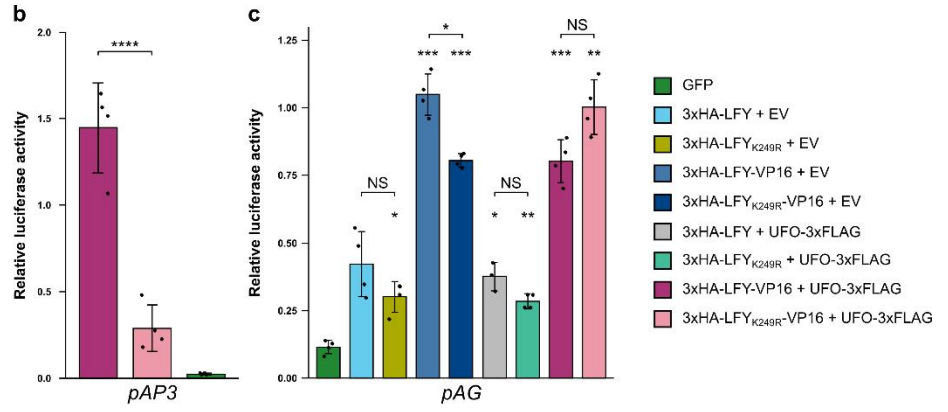
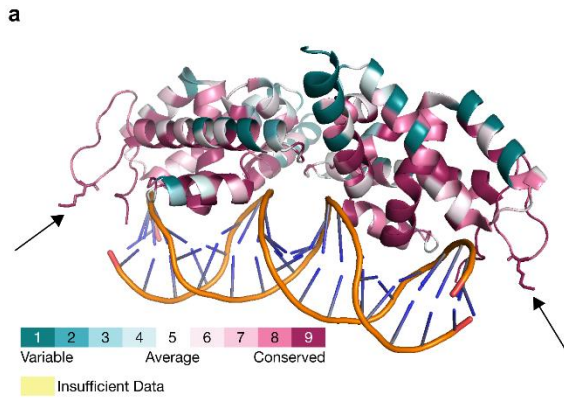
b



c

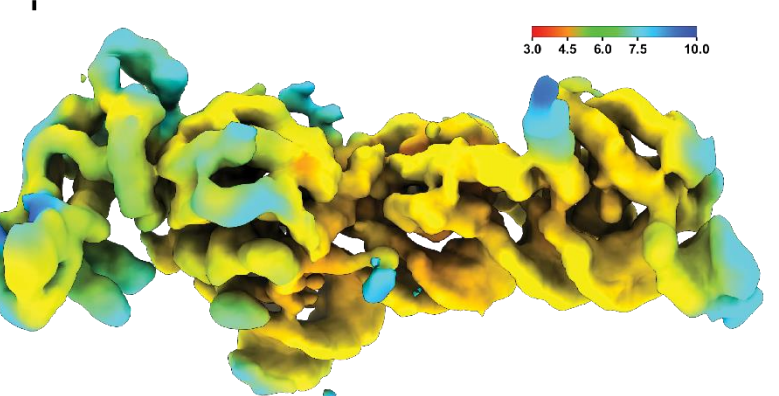
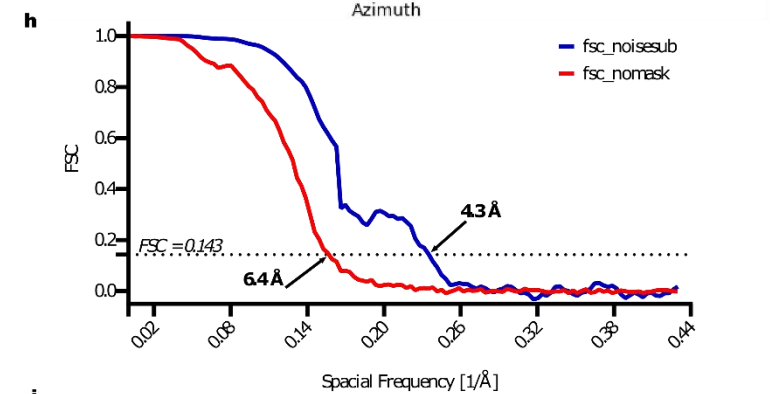
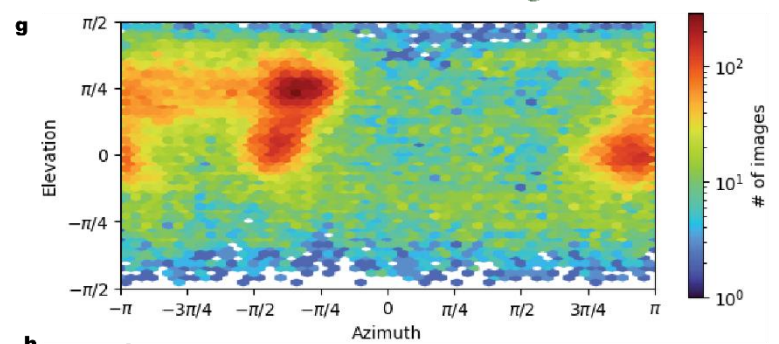
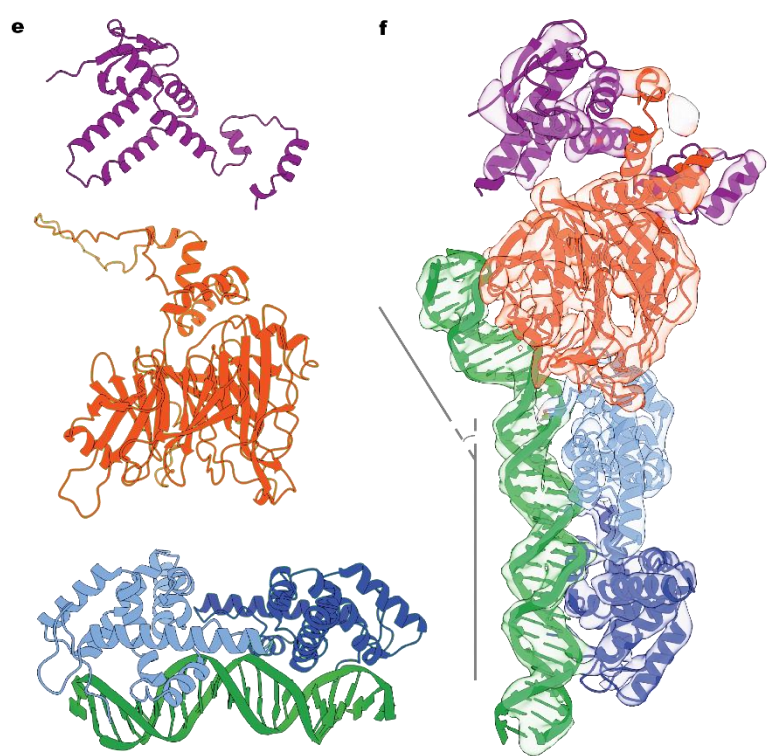
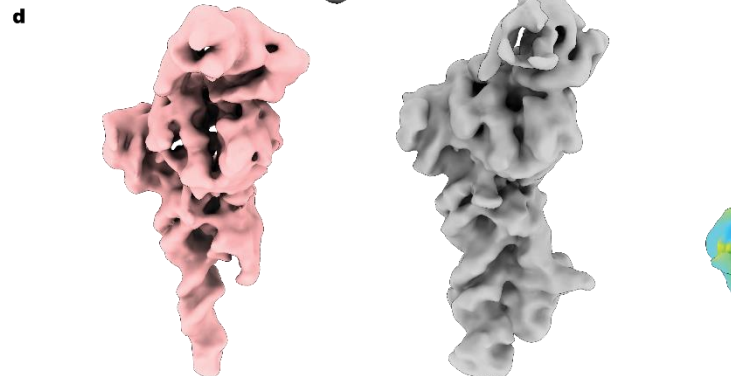
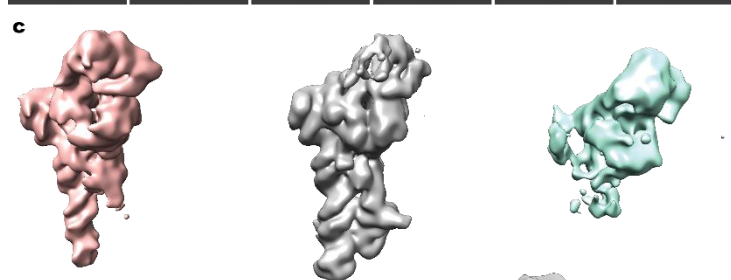
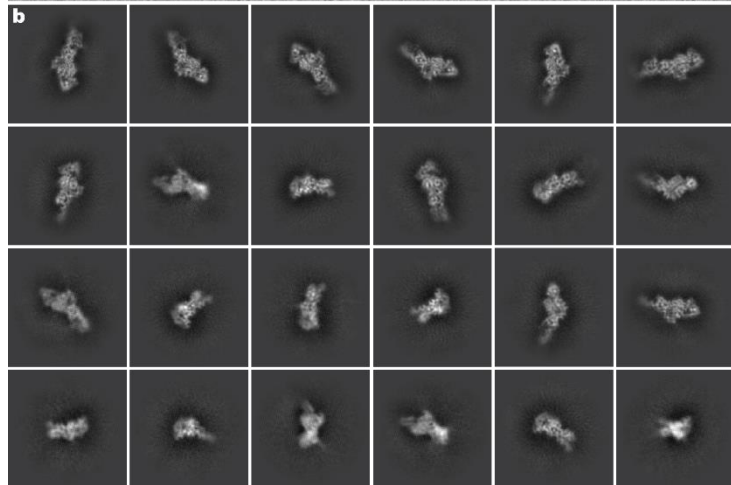
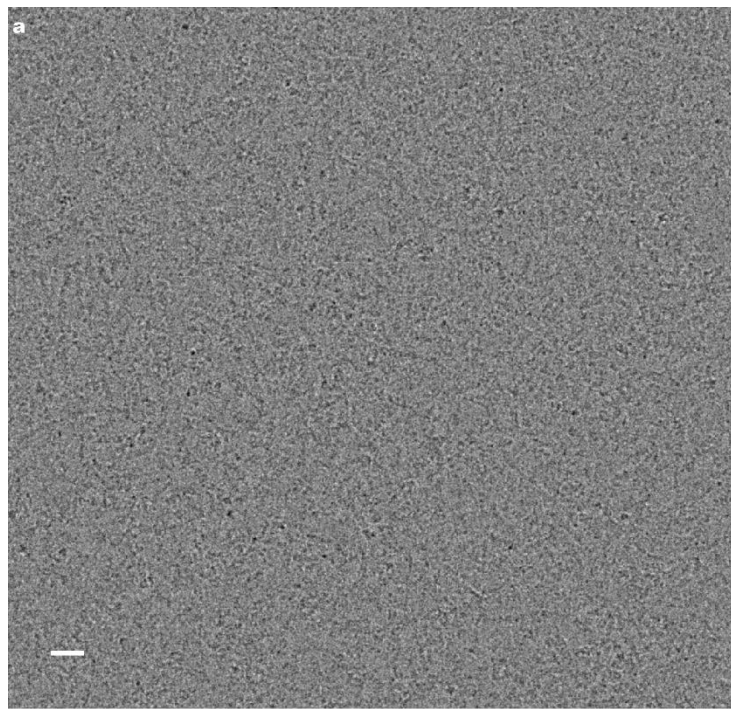


976 **Extended Data Fig. 7. LFY and UFO likely regulate other genes in Arabidopsis. a**, List of
977 candidate LFY-UFO target genes selected as i) present in regions specifically bound by LFY-
978 UFO in ampDAP-seq (high CFC) ii) bound *in vivo* in LFY ChIP-seq experiments (A²⁵; B²⁶;
979 C⁶⁸; D⁷⁰) and iii) deregulated in *ufo* inflorescences⁶⁹. **b**, IGB view of *PISTILLATA* promoter
980 region showing LFY ChIP-seq in inflorescences (light blue)²⁵ or seedlings (dark blue)²⁶, LFY-
981 UFO ampDAP-seq (yellow), LFY ampDAP-seq (pink)²⁷, numbers indicate read number range
982 (top). Predicted binding sites using the dLUBS, mLUBS models from Fig. 2e and LFY PWM
983 with dependencies⁶⁸, y-axis represents score values (bottom). **c**, IGB view of selected genes
984 showing LFY ChIP-seq in inflorescences (light blue)²⁵, LFY-UFO ampDAP-seq (yellow), LFY
985 ampDAP-seq (pink)²⁷, numbers indicate read number range. Genes in red are deregulated in
986 *ufo* inflorescences⁶⁹. ChIP-seq peaks better explained by LFY-UFO than by LFY alone are
987 shaded in grey.
988



990 **Extended Data Fig. 8. The LFY K249 is essential for LFY-UFO-LUBS complex formation.**
991 **a**, Structure of LFY-DBD³⁰. Residues were colored by conservation using ConSurf with default
992 parameters⁸⁰. K249 residues on each LFY monomer are represented as sticks and indicated with
993 arrows. Note that the K249-containing loop is highly conserved. **b,c**, Promoter activation
994 measured by DLRA in Arabidopsis protoplasts with indicated effectors (right). EV = Empty
995 Vector (pRT104-3xHA). Tested promoters are indicated below each graph. Note that for 3xHA-
996 LFY+UFO-3xFLAG on *pAG* only n = 3 biological replicates are shown. Data represent
997 averages of independent biological replicates and are presented as mean ± SD, each dot
998 representing one biological replicate (n = 4 unless specified). One-way ANOVA with Tukey's
999 multiple comparisons tests (**b**) or Welch's ANOVA with Games-Howell post-hoc test (**c**). In
1000 (**c**), stars above bars represent a statistical difference compared to GFP. Other comparisons are
1001 indicated with brackets. (NS: p > 0.05, *: p < 0.05, **: p < 0.01, ***: p < 0.001 and ****: p <
1002 0.0001). **d**, Effect of the LFY_{K249R} mutation on LFY-UFO interaction in Y2H. EV = Empty
1003 Vector. LFY-40 is a LFY version lacking the first 40 aa and better tolerated by yeast cells.
1004 Values correspond to the different dilutions (OD = 7, 0.7 and 0.07). Top picture corresponds to
1005 the non-selective plate lacking Leucine and Tryptophan (SD -L-W), and bottom picture
1006 corresponds to the selective plate lacking Leucine, Tryptophan, Histidine and Adenine (SD -L-
1007 W-A-H). Pictures were taken at day + 4. **e**, EMSA with DNA probes corresponding to *pAP3*
1008 DEE LFYBS and *pAP3* LUBS1 and indicated proteins. *pAP3* DEE LFYBS DNA probe was
1009 used as a control for binding on canonical LFYBS. **f**, WB after DNA elution during ampDAP-
1010 seq experiment. After DNA elution, 20 μL of 1X SDS-PAGE Protein Sample Buffer was added
1011 to the remaining beads to run WB. Each lane represents one replicate. **g**, Reproducibility of
1012 ampDAP-seq experiments with LFY_{K249R} (left) and LFY_{K249R}-UFO (right) through the
1013 comparison of replicates datasets 2 by 2. **h**, Comparison of peak coverage in LFY_{K249R} (y-axis,
1014 this study) and LFY (x-axis)²⁷ ampDAP-seq experiments. **i**, Integrated Genome Browser (IGB)

1015 view of *pAP3* showing LFY ChIP-seq in inflorescences (light blue)²⁵ or seedlings (dark blue)²⁶,
1016 LFY-UFO ampDAP-seq (yellow; this study), LFY ampDAP-seq (pink)²⁷ and LFY_{K249R}
1017 ampDAP-seq (purple; this study). Numbers indicate read number range. **j**, Pictures of WT and
1018 representative transgenic plants expressing *35S::LFY* or *35S::LFY_{K249R}* (scale bar, 1 cm). The
1019 white arrows indicate ectopic rosette flowers. *35S::LFY* was obtained previously²⁶. 42 T1 plants
1020 expressing *35S::LFY_{K249R}* were analyzed; the percentage of plants with a LFY overexpressing
1021 phenotype is comparable to the one obtained with *35S::LFY*²⁶.
1022



1024 **Extended Data Fig. 9. UFO binds DNA and LFY DBD. a,** A representative micrograph of
1025 the ASK1-UFO-LFY-DNA complex in vitreous ice (scale bar, 20 nm). **b,** Selected 2D class
1026 averages of the particles submitted to *ab initio* reconstruction and heterogeneous refinement for
1027 3D classification. **c,** Intermediate reconstructions of the 3D classes after heterogeneous
1028 refinement. **d,** Final reconstructions of ASK1-UFO-LFY-DNA complexes (involving either a
1029 LFY-DBD monomer (pink) or a LFY-DBD dimer (gray)) after Non-Uniform refinement. **e,**
1030 Unprocessed AlphaFold2 model for ASK1 (top, purple; uniprot ID, Q39255), UFO (middle,
1031 red; uniprot ID, Q39090) and the LFY-DBD dimer/DNA crystallographic structure (bottom,
1032 pale and dark blue for the LFY-DBD dimer and green for the DNA; PDB, 2VY1). **f,** Cryo-EM
1033 density map color-coded by fitted molecule. Note the kink on DNA induced by the presence of
1034 UFO. **g,** Heat map of the angular distribution of particle projections contributing for the final
1035 reconstruction of the complete ASK1-UFO-LFY-DNA complex (with a LFY-DBD dimer). **h,**
1036 Gold-standard Fourier shell correlation (FSC) curves. The dotted line represents the 0.143 FSC
1037 threshold, which indicates a nominal resolution of 6.4 Å for the unmasked (red) and 4.3 Å for
1038 the masked (blue) reconstruction. **i,** View of the post-processed map of the complete ASK1-
1039 UFO-LFY-DNA complex, colored according to the local resolution.

1040

- 1041 1. Moyroud, E., Kusters, E., Monniaux, M., Koes, R. & Parcy, F. LEAFY blossoms.
1042 *Trends in Plant Science* vol. 15 346–352 (2010).
- 1043 2. Irish, V. F. The flowering of Arabidopsis flower development. *Plant J.* **61**, 1014–1028
1044 (2010).
- 1045 3. Parcy, F., Nilsson, O., Busch, M. A., Lee, I. & Weigel, D. A genetic framework for
1046 floral patterning. *Nature* **395**, 561–566 (1998).
- 1047 4. Wagner, D., Sablowski, R. W. M. & Meyerowitz, E. M. Transcriptional activation of
1048 APETALA1 by LEAFY. *Science* **285**, 582–584 (1999).
- 1049 5. Lohmann, J. U. *et al.* A molecular link between stem cell regulation and floral
1050 patterning in Arabidopsis. *Cell* **105**, 793–803 (2001).
- 1051 6. Lee, I., Wolfe, D. S., Nilsson, O. & Weigel, D. A LEAFY co-regulator encoded by
1052 UNUSUAL FLORAL ORGANS. *Curr. Biol.* **7**, 95–104 (1997).
- 1053 7. Levin, J. Z. & Meyerowitz, E. M. UFO: an Arabidopsis gene involved in both floral
1054 meristem and floral organ development. *Plant Cell* **7**, 529–548 (1995).
- 1055 8. Wilkinson & Haughn. UNUSUAL FLORAL ORGANS Controls Meristem Identity
1056 and Organ Primordia Fate in Arabidopsis. *Plant Cell* **7**, 1485–1499 (1995).
- 1057 9. Krizek, B. A. & Meyerowitz, E. M. The Arabidopsis homeotic genes APETALA3 and
1058 PISTILLATA are sufficient to provide the B class organ identity function.
1059 *Development* **122**, 11–22 (1996).
- 1060 10. Ikeda-Kawakatsu, K., Maekawa, M., Izawa, T., Itoh, J.-I. & Nagato, Y. ABERRANT
1061 PANICLE ORGANIZATION 2/RFL, the rice ortholog of Arabidopsis LEAFY,
1062 suppresses the transition from inflorescence meristem to floral meristem through
1063 interaction with APO1. *Plant J.* **69**, 168–180 (2012).

- 1064 11. Lippman, Z. B. *et al.* The Making of a Compound Inflorescence in Tomato and Related
1065 Nightshades. *PLoS Biol.* **6**, e288 (2008).
- 1066 12. Souer, E. *et al.* Patterning of Inflorescences and Flowers by the F-Box Protein
1067 DOUBLE TOP and the LEAFY Homolog ABERRANT LEAF AND FLOWER of
1068 Petunia. *Plant Cell Online* **20**, 2033–2048 (2008).
- 1069 13. Kuzay, S. *et al.* WAPO-A1 is the causal gene of the 7AL QTL for spikelet number per
1070 spike in wheat. *PLoS Genet.* **18**, (2022).
- 1071 14. Ingram, G. C. *et al.* Dual role for fimbriata in regulating floral homeotic genes and cell
1072 division in Antirrhinum. *EMBO J.* **16**, 6521–6534 (1997).
- 1073 15. Samach, A. *et al.* The UNUSUAL FLORAL ORGANS gene of Arabidopsis thaliana is
1074 an F-box protein required for normal patterning and growth in the floral meristem.
1075 *Plant J.* **20**, 433–445 (1999).
- 1076 16. Simon, R., Carpenter, R., Doyle, S. & Coen, E. Fimbriata controls flower development
1077 by mediating between meristem and organ identity genes. *Cell* **78**, 99–107 (1994).
- 1078 17. Wang, X. *et al.* The COP9 Signalosome Interacts with SCF UFO and Participates in
1079 Arabidopsis Flower Development. *Plant Cell* **15**, 1071–1082 (2003).
- 1080 18. Chae, E., Tan, Q. K.-G., Hill, T. A. & Irish, V. F. An Arabidopsis F-box protein acts as
1081 a transcriptional co-factor to regulate floral development. *Development* **135**, 1235–
1082 1245 (2008).
- 1083 19. Geng, F., Wenzel, S. & Tansey, W. P. Ubiquitin and Proteasomes in Transcription.
1084 *Annu. Rev. Biochem.* **81**, 177–201 (2012).
- 1085 20. Risseuw, E. *et al.* An activated form of UFO alters leaf development and produces
1086 ectopic floral and inflorescence meristems. *PLoS One* **8**, (2013).

- 1087 21. Busch, M. A., Bomblies, K. & Weigel, D. Activation of a floral homeotic gene in
1088 Arabidopsis. *Science* **285**, 585–587 (1999).
- 1089 22. Krizek, B. A., Lewis, M. W. & Fletcher, J. C. *RABBIT EARS* is a second-whorl
1090 repressor of *AGAMOUS* that maintains spatial boundaries in Arabidopsis flowers. *Plant*
1091 *J.* **45**, 369–383 (2006).
- 1092 23. Hill, T. A., Day, C. D., Zondlo, S. C., Thackeray, A. G. & Irish, V. F. Discrete spatial
1093 and temporal cis-acting elements regulate transcription of the Arabidopsis floral
1094 homeotic gene *APETALA3*. *Development* **125**, 1711–1721 (1998).
- 1095 24. Lamb, R. S., Hill, T. a, Tan, Q. K.-G. & Irish, V. F. Regulation of *APETALA3* floral
1096 homeotic gene expression by meristem identity genes. *Development* **129**, 2079–2086
1097 (2002).
- 1098 25. Goslin, K. *et al.* Transcription Factor Interplay between *LEAFY* and
1099 *APETALA1/CAULIFLOWER* during Floral Initiation. *Plant Physiol.* **174**, 1097–1109
1100 (2017).
- 1101 26. Sayou, C. *et al.* A SAM oligomerization domain shapes the genomic binding landscape
1102 of the *LEAFY* transcription factor. *Nat. Commun.* **7**, 11222 (2016).
- 1103 27. Lai, X. *et al.* The *LEAFY* floral regulator displays pioneer transcription factor
1104 properties. *Mol. Plant* **14**, 829–837 (2021).
- 1105 28. Weigel, D., Alvarez, J., Smyth, D. R., Yanofsky, M. F. & Meyerowitz, E. M. *LEAFY*
1106 controls floral meristem identity in *Arabidopsis*. *Cell* **69**, 843–859 (1992).
- 1107 29. Weigel, D. & Nilsson, O. A developmental switch sufficient for flower initiation in
1108 diverse plants. *Nature* **377**, 495–500 (1995).
- 1109 30. Hamès, C. *et al.* Structural basis for *LEAFY* floral switch function and similarity with

- 1110 helix-turn-helix proteins. *EMBO J.* **27**, 2628–2637 (2008).
- 1111 31. Sayou, C. *et al.* A promiscuous intermediate underlies the evolution of LEAFY DNA
1112 binding specificity. *Science* **343**, 645–648 (2014).
- 1113 32. Zhao, D., Yu, Q., Chen, M. & Ma, H. The ASK1 gene regulates B function gene
1114 expression in cooperation with UFO and LEAFY in Arabidopsis. *Development* **128**,
1115 2735–2746 (2001).
- 1116 33. Ni, W. *et al.* Regulation of flower development in arabidopsis by SCF complexes.
1117 *Plant Physiol.* **134**, 1574–1585 (2004).
- 1118 34. Levin, J. Z., Fletcher, J. C., Chen, X. & Meyerowitz, E. M. A genetic screen for
1119 modifiers of UFO meristem activity identifies three novel FUSED FLORAL ORGANS
1120 genes required for early flower development in Arabidopsis. *Genetics* **149**, 579–595
1121 (1998).
- 1122 35. Singh, N. & Bhalla, N. Moonlighting Proteins. (2020) doi:10.1146/annurev-genet-
1123 030620.
- 1124 36. Honma, T. & Goto, K. *PISTILLATA transcriptional regulation.* (2000).
- 1125 37. Tilly, J. J., Allen, D. W. & Jack, T. The CArG boxes in the promoter of the
1126 Arabidopsis floral organ identity gene APETALA3 mediate diverse regulatory effects.
1127 *Development* **125**, 1647–1657 (1998).
- 1128 38. Liu, C., Xi, W., Shen, L., Tan, C. & Yu, H. Regulation of floral patterning by flowering
1129 time genes. *Dev. Cell* **16**, 711–22 (2009).
- 1130 39. Gregis, V., Sessa, A., Colombo, L. & Kater, M. M. AGL24 , SHORT VEGETATIVE
1131 PHASE , and APETALA1 Redundantly Control AGAMOUS during Early Stages of
1132 Flower Development in Arabidopsis. *Plant Cell* **18**, 1373–1382 (2006).

- 1133 40. Castillejo, C., Romera-Branchat, M. & Pelaz, S. A new role of the Arabidopsis
1134 SEPALLATA3 gene revealed by its constitutive expression. *Plant J.* **43**, 586–596
1135 (2005).
- 1136 41. Siggers, T., Duyzend, M. H., Reddy, J., Khan, S. & Bulyk, M. L. Non-DNA-binding
1137 cofactors enhance DNA-binding specificity of a transcriptional regulatory complex.
1138 *Mol. Syst. Biol.* **7**, 555 (2011).
- 1139 42. Babb, R., Huang, C., Aufiero, D. J. & Herr, W. DNA Recognition by the Herpes
1140 Simplex Virus Transactivator VP16: a Novel DNA-Binding Structure. *Mol. Cell. Biol.*
1141 **21**, 4700–4712 (2001).
- 1142 43. Chahtane, H. *et al.* LEAFY activity is post-transcriptionally regulated by BLADE ON
1143 PETIOLE2 and CULLIN3 in Arabidopsis. *New Phytol.* **220**, 579–592 (2018).
- 1144 44. Blanvillain, R. *et al.* The Arabidopsis peptide kiss of death is an inducer of
1145 programmed cell death. *EMBO J.* **30**, 1173–1183 (2011).
- 1146 45. Takeda, S., Matsumoto, N. & Okada, K. RABBIT EARS, encoding a SUPERMAN-
1147 like zinc finger protein, regulates petal development in Arabidopsis thaliana.
1148 *Development* **131**, 425–34 (2004).
- 1149 46. Benlloch, R. *et al.* Integrating long-day flowering signals: A LEAFY binding site is
1150 essential for proper photoperiodic activation of APETALA1. *Plant J.* **67**, 1094–1102
1151 (2011).
- 1152 47. Iwata, Y., Lee, M. H. & Koizumi, N. Analysis of a transcription factor using transient
1153 assay in Arabidopsis protoplasts. *Methods Mol. Biol.* **754**, 107–117 (2011).
- 1154 48. Dümmler, A., Lawrence, A. M. & de Marco, A. Simplified screening for the detection
1155 of soluble fusion constructs expressed in E. coli using a modular set of vectors. *Microb.*

- 1156 *Cell Fact.* **4**, 34 (2005).
- 1157 49. Bartlett, A. *et al.* Mapping genome-wide transcription-factor binding sites using DAP-
1158 seq. *Nat. Protoc.* **12**, 1659–1672 (2017).
- 1159 50. Cutler, S. R., Ehrhardt, D. W., Griffiths, J. S. & Somerville, C. R. Random GFP::cDNA
1160 fusions enable visualization of subcellular structures in cells of Arabidopsis at a high
1161 frequency. *Proc. Natl. Acad. Sci. U. S. A.* **97**, 3718 (2000).
- 1162 51. Chahtane, H. *et al.* A variant of LEAFY reveals its capacity to stimulate meristem
1163 development by inducing *RAX1*. *Plant J.* **74**, 678–689 (2013).
- 1164 52. Punjani, A., Rubinstein, J. L., Fleet, D. J. & Brubaker, M. A. cryoSPARC: algorithms
1165 for rapid unsupervised cryo-EM structure determination. *Nat. Methods* 2017 143 **14**,
1166 290–296 (2017).
- 1167 53. Wagner, T. *et al.* SPHIRE-crYOLO is a fast and accurate fully automated particle
1168 picker for cryo-EM. *Commun. Biol.* 2019 21 **2**, 1–13 (2019).
- 1169 54. Punjani, A., Zhang, H. & Fleet, D. J. Non-uniform refinement: adaptive regularization
1170 improves single-particle cryo-EM reconstruction. *Nat. Methods* 2020 1712 **17**, 1214–
1171 1221 (2020).
- 1172 55. Sanchez-Garcia, R. *et al.* DeepEMhancer: a deep learning solution for cryo-EM
1173 volume post-processing. *Commun. Biol.* 2021 41 **4**, 1–8 (2021).
- 1174 56. Pettersen, E. F. *et al.* UCSF Chimera--a visualization system for exploratory research
1175 and analysis. *J. Comput. Chem.* **25**, 1605–1612 (2004).
- 1176 57. Pettersen, E. F. *et al.* UCSF ChimeraX: Structure visualization for researchers,
1177 educators, and developers. *Protein Sci.* **30**, 70–82 (2021).

- 1178 58. Emsley, P., Lohkamp, B., Scott, W. G. & Cowtan, K. Features and development of
1179 Coot. *Acta Crystallogr. D. Biol. Crystallogr.* **66**, 486–501 (2010).
- 1180 59. Afonine, P. V. *et al.* Real-space refinement in PHENIX for cryo-EM and
1181 crystallography. *Acta Crystallogr. Sect. D, Struct. Biol.* **74**, 531 (2018).
- 1182 60. Jumper, J. *et al.* Highly accurate protein structure prediction with AlphaFold. *Nat.* 2021
1183 5967873 **596**, 583–589 (2021).
- 1184 61. Terwilliger, T. C. *et al.* Improved AlphaFold modeling with implicit experimental
1185 information. *bioRxiv* 2022.01.07.475350 (2022) doi:10.1101/2022.01.07.475350.
- 1186 62. Lai, X. *et al.* Genome-wide binding of SEPALLATA3 and AGAMOUS complexes
1187 determined by sequential DNA-affinity purification sequencing. *Nucleic Acids Res.* **48**,
1188 9637–9648 (2020).
- 1189 63. Gaspar, J. M. NGmerge: merging paired-end reads via novel empirically-derived
1190 models of sequencing errors. *BMC Bioinformatics* **19**, 536 (2018).
- 1191 64. Berardini, T. Z. *et al.* The Arabidopsis Information Resource: Making and Mining the
1192 ‘Gold Standard’ Annotated Reference Plant Genome. *Genesis* **53**, 474 (2015).
- 1193 65. Jalili, V., Matteucci, M., Masseroli, M. & Morelli, M. J. Using combined evidence
1194 from replicates to evaluate ChIP-seq peaks. *Bioinformatics* **31**, 2761–2769 (2015).
- 1195 66. Machanick, P. & Bailey, T. L. MEME-ChIP: motif analysis of large DNA datasets.
1196 *Bioinformatics* **27**, 1696–1697 (2011).
- 1197 67. Stigliani, A. *et al.* Capturing Auxin Response Factors Syntax Using DNA Binding
1198 Models. *Mol. Plant* **12**, 822–832 (2019).
- 1199 68. Moyroud, E. *et al.* Prediction of Regulatory Interactions from Genome Sequences

- 1200 Using a Biophysical Model for the *Arabidopsis* LEAFY Transcription Factor. *Plant*
1201 *Cell* **23**, 1293–1306 (2011).
- 1202 69. Schmid, M. *et al.* A gene expression map of *Arabidopsis thaliana* development. *Nat.*
1203 *Genet.* 2005 375 **37**, 501–506 (2005).
- 1204 70. Jin, R. *et al.* LEAFY is a pioneer transcription factor and licenses cell reprogramming
1205 to floral fate. *Nat. Commun.* 2021 121 **12**, 1–14 (2021).
- 1206 71. Gagne, J. M., Downes, B. P., Shiu, S. H., Durski, A. M. & Vierstra, R. D. The F-box
1207 subunit of the SCF E3 complex is encoded by a diverse superfamily of genes in
1208 *Arabidopsis*. *Proc. Natl. Acad. Sci. U. S. A.* **99**, 11519–11524 (2002).
- 1209 72. Zhang, S. *et al.* Proliferating floral organs (pfo), a *Lotus japonicus* gene required for
1210 specifying floral meristem determinacy and organ identity, encodes an F-box protein.
1211 *Plant J.* **33**, 607–619 (2003).
- 1212 73. Zhao, Y. *et al.* Evolutionary co-option of floral meristem identity genes for patterning
1213 of the flower-like asteraceae inflorescence. *Plant Physiol.* **172**, 284–296 (2016).
- 1214 74. Chen, Y. *et al.* CsUFO is involved in the formation of flowers and tendrils in
1215 cucumber. *Theor. Appl. Genet.* **3**, (2021).
- 1216 75. Ikeda, K., Ito, M., Nagasawa, N., Kyojuka, J. & Nagato, Y. Rice ABERRANT
1217 PANICLE ORGANIZATION 1, encoding an F-box protein, regulates meristem fate.
1218 *Plant J.* **51**, 1030–1040 (2007).
- 1219 76. Li, F. *et al.* Reduced expression of CbUFO is associated with the phenotype of a
1220 flower-defective *cosmos bipinnatus*. *Int. J. Mol. Sci.* **20**, 2503 (2019).
- 1221 77. Sasaki, K. *et al.* Mutation in *Torenia fournieri* Lind. UFO homolog confers loss of
1222 TFLFY interaction and results in a petal to sepal transformation. *Plant J.* **71**, 1002–

1223 1014 (2012).

1224 78. Sharma, B. *et al.* Homologs of LEAFY and UNUSUAL FLORAL ORGANS Promote
1225 the Transition From Inflorescence to Floral Meristem Identity in the Cymose *Aquilegia*
1226 *coerulea*. *Front. Plant Sci.* **10**, (2019).

1227 79. Taylor, S., Hofer, J. & Murfet, I. Stamina pistilloida, the pea ortholog of Fim and UFO,
1228 is required for normal development of flowers, inflorescences, and leaves. *Plant Cell*
1229 **13**, 31–46 (2001).

1230 80. Ashkenazy, H. *et al.* ConSurf 2016: an improved methodology to estimate and
1231 visualize evolutionary conservation in macromolecules. *Nucleic Acids Res.* **44**, W344–
1232 W350 (2016).

1233

1234

1235

1236